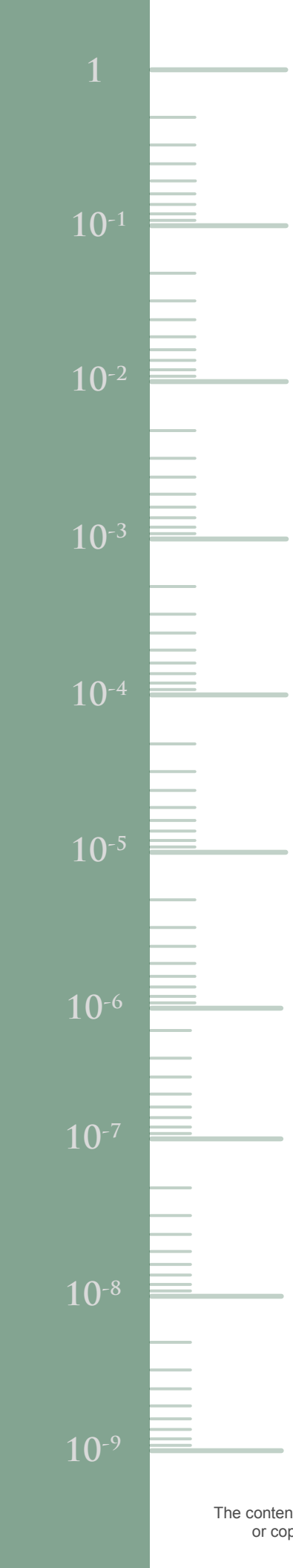

NCL
Nanotechnology
Characterization
Laboratory

NCL201304A

Characterization of Nanocurcumin

prepared for

Dr. Anirban Maitra,
Johns Hopkins University
&
Dr. Lawrence Helson,
SignPath Pharma, Inc.

Nanotechnology Characterization Laboratory
Frederick National Laboratory for Cancer Research
SAIC-Frederick, Inc.
Frederick, MD 21702
(301) 846-6939 • ncl@mail.nih.gov
http://ncl.cancer.gov

Nanocurcumin....3

Note: The protocols for NCL characterizations are denoted by three letter acronyms and numbers (e.g. PCC-1, STE-1, or ITA-5, etc.). Detailed descriptions of these protocols can be found on the NCL website: http://ncl.cancer.gov/working_assay-cascade.asp

Nanocurcumin

Objective

The objective of the NCL – SignPath Pharma collaboration was characterization of their nanoformulation of curcumin. NCL provided endotoxin analysis, hydrodynamic size and zeta potential measurements, in vitro cytotoxicity and immunological assays, as well as drug metabolism and pharmacokinetic studies.

This report details the characterization of SignPath Pharma's nanoformulation of curcumin, NCL150, as well as the void polymer platform (i.e. no curcumin), NCL149. Details on the lots of materials received by the NCL are listed below.

NCL149-1: Void Polymer (acrylic acid and vinyl pyrrolidinone)
Sponsor Lot Number: VP#C
Date Received: March 11, 2009
Quantity Received: ~100 mg

NCL150: Nanocurcumic

NCL150-1
Sponsor Lot Number: NC#A
Date Received: March 11, 2009
Quantity Received: ~100 mg

NCL150-2
Sponsor Lot Number: NC#B
Date Received: March 11, 2009
Quantity Received: ~100 mg
Note: Also has free curcumin

NCL150-3
Sponsor Lot Number: P227-32-2
Date Received: June 14, 2011
Quantity Received: 6 x 1 mg

NCL150-3
Sponsor Lot Number: P227-32-2
Date Received: August 31, 2011
Quantity Received: 50 g
Note: same lot as previous submission

Lots #1 and #2 of the nanocurcumin were utilized in the prescreen characterization only, i.e. sterility, endotoxin, hydrodynamic size, and zeta potential. Only NCL150-3 was used further in the in vitro and in vivo analyses.

Note: Throughout this report, concentrations are denoted either as mg nanocurcumin, i.e. the weight of the total formulation, or as mg curcumin, the weight of the API only.

Executive Summary

Curcumin is a natural diphenolic compound derived from turmeric (*Curcuma longa*), which is currently undergoing evaluation as a chemopreventive and anticancer agent [1]. NCL characterization of SignPath Pharma's nanocurcumin formulation (NCL150) included a range of assays including physicochemical characterization, in vitro cytotoxicity and immunological assays, and a drug metabolism and pharmacokinetics study in rodents. An overview of the results from these analyses is presented here. Details of each experimental method and further discussions on the analyses are provided in the subsequent sections.

Sterility and Endotoxin

The purpose of these studies was to assess sterility and pyrogenicity. Both the void polymer, NCL149, as well as the nanocurcumin formulation, NCL150, were free from bacterial, yeast, and mold contamination. Endotoxin levels were varied for different lots of the material, but were over the USP acceptable allowance of 5 EU/kg. The materials were also tested by rabbit pyrogen test and macrophage activation test for pyrogenicity; these assays showed NCL150 was not pyrogenic.

Physicochemical Characterization

The physicochemical characterization of nanocurcumin and its control, void polymer included only dynamic light scattering (DLS) for size/size distribution (hydrodynamic diameter) and zeta potential for surface charge assessment. NCL149, the void polymer displayed a bimodal size distribution with the major peak at ~14 nm, and a minor size population from 100-1000 nm. NCL150, the curcumin encapsulated polymer, i.e. nanocurcumin, also displayed a bimodal size distribution, but with peaks at ~10 nm and ~88 nm. The majority of the sample, however, corresponds to the ~10 nm peak. The zeta potentials for both NCL149 and NCL150 were negative, with NCL149 at -13 mV and NCL150 at -17mV.

In Vitro Cytotoxicity

The in vitro cytotoxicity of nanocurcumin, NCL150, was evaluated against human hepatocarcinoma (HepG2) and porcine renal proximal tubule (LLC-PK1) cell lines, in comparison to DMSO-solubilized curcumin. Both cell lines evaluated were similarly sensitive to NCL150 and the DMSO-solubilized curcumin. The 48 h IC_{50} values were determined by the MTT assay. NCL150 displayed an IC_{50} of 0.012 mM and 0.036 mM for HepG2 and LLC-PK1 cell lines, respectively. DMSO-solubilized curcumin displayed an IC_{50} of 0.59 mM and 0.25 mM (estimated from partial response), for HepG2 and LLC-PK1 cell lines, respectively.

In Vitro Immunological Characterization

In vitro immunological evaluation of NCL150 included assessment of hematocompatibility and possible effects on immune cell functions. Under the tested assay conditions, NCL150 was not hemolytic, did not induce platelet aggregation, did not change plasma coagulation time, did not induce leukocyte proliferation, did not activate the human complement system, was not chemoattractive, and did not induce NO^- secretion *in vitro*. At the highest tested concentrations (21 mg/mL) NCL150 suppressed collagen-induced platelet aggregation and mitogen- and antigen-induced leukocyte proliferation, and inhibited NK cytotoxicity, LPS-induced pyrogenic

cytokines (IL-1β, TNFα) and IFNγ. NCL150 treatment also induced IL-8 secretion as well as enhanced IL-8 secretion induced by endotoxin. Some immunosuppressive properties of NCL150 (i.e. antigen-induced leukocyte proliferation) were attributed to the polymeric component of the formulation, as the same effect was observed with NCL149, the void polymer.

In Vivo Drug Metabolism and Pharmacokinetics
Free, unencapsulated curcumin is rapidly metabolized and excreted in rats. This metabolic instability was utilized to assess *in vivo* drug (curcumin) release from nanocurcumin. Upon i.v. administration of nanocurcumin (NCL150), only nanoparticle encapsulated curcumin can be detected in plasma samples. Measured curcumin concentrations were assumed part of the nanoformulation and were used to estimate the concentration of the nanocurcumin formulation. Metabolite concentrations were used to estimate the concentration of any unencapsulated curcumin. In addition, the in vivo study was used to compare the pharmacokinetics of nanocurcumin to a DMSO-solubilized curcumin.

The nanoformulation of curcumin increased the C_{max} more than 1000-fold in plasma. However, the nanocurcumin in plasma only accounted for approximately 10% of the injected dose, and significantly increased the excretion of curcumin and metabolites in bile and urine. This suggests a rapid, “burst” release of curcumin. Nanoformulation of curcumin, however, does not significantly accumulate in the lung, as the DMSO-solubilized curcumin does.

I. Sterility & Endotoxin

Section Summary

The purpose of this study was to test nanocurcumin sterility, endotoxin contamination, and pyrogenicity. The sterility of the samples (NCL149, the void polymer, as well as several batches of NCL150, the nanocurcumin formulation) was assessed by plating samples on an agar plate. All samples were deemed free of bacterial, yeast, and mold contamination under the tested assay conditions. These formulation as well as several components from the synthetic process were tested for endotoxin contamination by the kinetic turbidity Limulus Amoebocyte Lysate (LAL) assay. The highest level of endotoxin detected was 1 EU/mg in NCL150-3 (Table I-1). Since the endotoxin data was so variable between lots, and given that at the mouse therapeutic dose the endotoxin levels would be above those acceptable by USP guidelines (5 EU/kg), pyrogenicity was also assessed by a rabbit pyrogen test (RPT) and macrophage activation test (MAT).

Under the tested assay conditions, the materials were not deemed pyrogenic by either the RPT (Table I-2) or the MAT (Figure I-1). However, it is worth noting that several other assays performed (see discussion in Section IV) suggest the formulation may have immunosuppressive properties. In this case, these immunosuppressive properties, if present, could negate pyrogenic responses

Sterility (STE-2.2)

Design and Methods

Both NCL149, the void polymer, and NCL150, the nanocurcumin polymer, were assessed for sterility. The sterility was assessed using NCL protocol STE-2.2 (http://ncl.cancer.gov/working_assay-cascade.asp), which plates samples on an agar plate and monitors growth. NCL149-1, NCL150-1, NCL150-2 and NCL150-3 were tested at a concentration of 1 mg/mL nanocurcumin (i.e. total formulation).

Results & Conclusions

No bacterial, yeast or mold contamination was detected in any of the tested formulations under the experimental conditions employed.

Endotoxin (STE-1.2)

Design and Methods

The purpose of this study was to test nanomaterial endotoxin contamination. Contamination with bacterial endotoxins was assessed following NCL protocol STE-1.2, the kinetic turbidity Limulus Amoebocyte Lysate (LAL) assay (http://ncl.cancer.gov/working_assay-cascade.asp).

Endotoxin contamination was assessed in NCL149-1, NCL150-1, NCL150-2 and NCL150-3, and in individual reagents used during the synthesis.

Results

Various levels of endotoxin were detected in NCL149-1 and the multiple batches of NCL150. NCL150-3 contained the highest level of endotoxin at 1.01 EU/mg. Endotoxin was also detected in the individual reagents curcumin, polymer-2 and vinylpyrrolidone; endotoxin was undetectable in other tested reagents. The data is summarized in Table I-1.

Table I-1. Endotoxin Results.

Sample	Turbidity LAL, EU/mg
NCL149-1	0.459
NCL150-1	0.772
NCL150-2	0.541
NCL150-3	1.01
Curcumin (supernatant)-1	0.263
DVP-1	<0.5
Acrylic Acid, lot #1	<0.5
DAA-1	<0.5
Polymer-2	1.52
Acrylic Acid, lot #2	<0.005
Vinylpyrrolidone-2	0.9
Isopropylacylamide-2	<0.005

Analysis and Conclusions

This data suggests inconsistency in the endotoxin levels between different batches of NCL150. This could be due to endotoxin or other LAL-reactive materials in the starting materials, specifically the polymer and curcumin. The intended dosing concentration of NCL150 is 25 mg/kg nanocurcumin in a mouse model, as established by the sponsor. NCL150, if used at this dose level, would be above the USP limit of 5 EU/kg. Therefore, we also performed rabbit pyrogen testing and an in vitro macrophage activation test to verify these LAL findings.

The endotoxin analysis was done using only the turbidity method because the nanocurcumin particles interfered with the gel-clot LAL. The chromogenic assay was not pursued because curcumin absorbance overlaps with the chromogenic LAL wavelength.

In Vivo Rabbit Pyrogen Test

Design and Methods

The objective of this experiment was to verify the pyrogenicity of the nanocurcumin formulation. If the LAL results were solely due to nanoparticle interference with the LAL assay, the rabbit pyrogen test (RPT) would be negative. If however, the material was contaminated with endotoxin, the RPT would be positive. Also, since RPT is not specific to endotoxin and detects other pyrogens, it was also expected to identify any inherent pyrogenic properties of the materials.

The study was conducted by WuxiAppTec (St. Paul, MN) according to the USP standard 151 "Pyrogen test". The nanoparticle formulation, NCL150-3, was reconstituted in sterile, pyrogen-free saline and injected into rabbits via ear vein at a final dose of 6 mg of nanocurcumin/kg. The dose was chosen using EU levels detected by the LAL assay (Table I-1), which would inject endotoxin levels slightly above the pyrogenic cut-off dose (5 EU/kg). If the LAL-reactive material was indeed endotoxin, administration of the material at its therapeutic dose of 25 mg/kg (as found in mice by the sponsor) would have been lethal to the animals. Further, the conversion of a mouse therapeutic dose into a rabbit therapeutic dose:

$$\frac{25 \text{ mg/kg}}{12.3} \times 3.1 = 6.3 \text{ mg/kg}$$

resulted in dose of ~6 mg/kg, where 12.3 is the factor used to convert a mouse dose to human and 3.1 is the factor used to convert a human dose to a rabbit dose.

Results

NCL150-3 did not result in elevation of body temperature >0.5°C above the baseline temperature in any of the three tested animals (Table I-2), and therefore, was considered non-pyrogenic.

Table I-2. Rabbit Pyrogen Test results. Three animals were injected via ear vein with 6 mg/kg of NCL150-3. Animals' body temperature was measured after 1 hour of injection and every 30 minutes thereafter, up to 3 hours post injection.

Animal #	**21891**	**18670**	**21893**
Weight (kg)	3.7	3.8	4.3
Dose (mL)	3.7	3.8	4.3
Baseline Temp (C)	**39.0**	**39.2**	**39.5**
1.0 hr Temp (C)	39.1	39.1	39.5
1.5 hr Temp (C)	39.1	39.0	39.5
2.0 hr Temp (C)	39.1	39.0	39.5
2.5 hr Temp (C)	39.0	38.9	39.3
3.0 hr Temp (C)	39.1	39.1	39.6
Max Temp Rise (C)	**0.1**	**0.0**[a]	**0.1**

[a]A negative difference in temperatures was reported as zero (0) temperature rise.

Analysis and Conclusions

Based on the guidelines of the USP standard, the material is not pyrogenic because all three animals failed to exhibit an increased body temperature above the baseline after injection. At first glance this data can be interpreted in support of LAL interference; however, other biological tests discussed in the immunological characterization section (Section IV of this report) suggest that the polymeric portion of the nanocurcumin formulation (i.e. NCL149-1) may have immunosuppressive properties. See Section IV for further discussion.

Although several reports have suggested an anti-inflammatory role for curcumin (1-8), the curcumin loading is very low (<1%) in NCL150. Thus, any potential immunosuppressive properties of NCL150 may be resulting from a different mechanism.

In vitro Macrophage Activation Test

Design and Methods

The objective of this experiment was to correlate the in vivo pyrogen response to in vitro pyrogenicity cytokine marker expression and to understand potential nanoparticle effects on the LPS-induced pyrogenicity cytokine marker. The Interagency Coordinating Committee on the Validation of Alternative Methods (ICCVAM) protocol validated by National Toxicology Program (NTP) (http://iccvam.niehs.nih.gov/docs/pyrogen/BRD/Appx-A5-2.pdf) was used for this assay.

NCL150-3 was tested at four concentrations (21, 2.1, 0.21 and 0.021 mg/mL nanocurcumin), of which 0.021 mg/mL is the theoretical blood concentration in human blood when this formulation is used at a dose equivalent to the 25 mg/kg efficacious dose established in mice by the sponsor. To calculate this concentration we first converted the mouse dose into a human dose (using 12 as an approximate mouse to human conversion factor):

$$25 \text{ mg/kg} \div 12 = 2.08 \text{ mg/kg}$$

Then, assuming that an average patient's weight is 70 kg and the blood volume is 7000 mL (~ 10% of body weight), and that all injected material will stay in circulation, the dose was calculated as follows:

$$2.08 \text{ mg/kg} \times 70 \text{ kg} = 145.8 \text{ mg in } 7000 \text{ mL of blood} = 0.021 \text{ mg/mL}$$

Results

Under the tested assay conditions, NCL150-3 did not induce IL-1β in MM-6 cells at the range of concentrations tested. NCL150-3 did, however, exhibit inhibition of cytokine induction by LPS at all tested concentrations (Figure I-1).

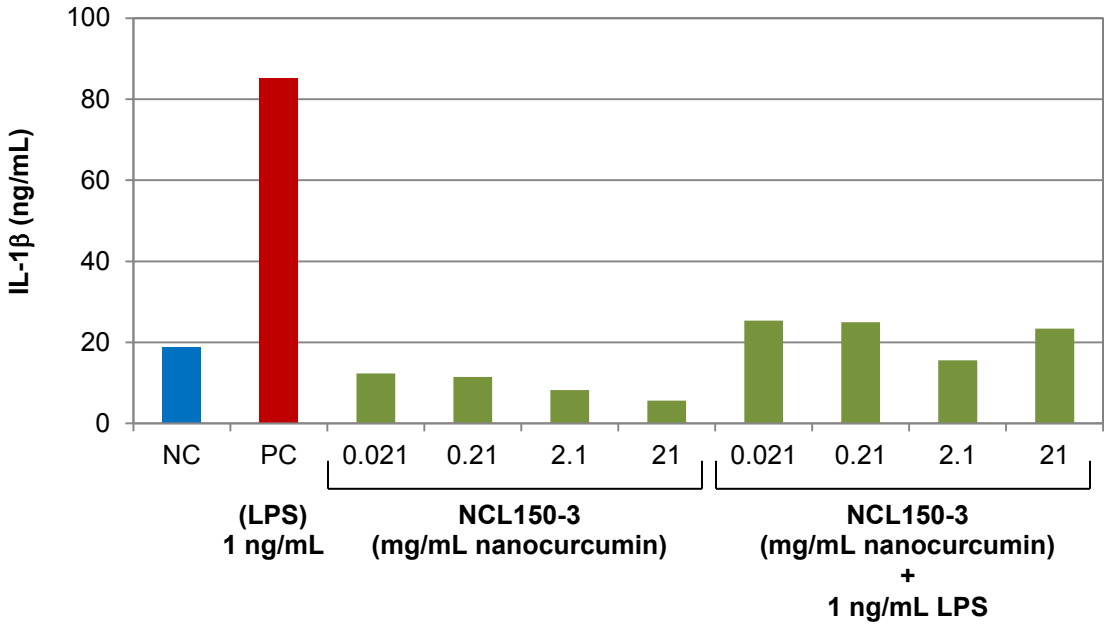

Figure I-1. Macrophage Activation Test. NCL150-3 was tested at four concentrations (0.021, 0.21, 2.1, and 21 mg/mL). MM-6 cells were treated with negative control (PBS; NC), positive control (PC; 1 ng/mL LPS), nanoparticles alone, or nanoparticles in combination with the positive control. Each bar represents the mean of duplicate results (%CV < 20). PBS was used to reconstitute nanoparticles and LPS.

Analysis and Conclusions

The results of this *in vitro* test are in agreement with the data obtained in the *in vivo* rabbit pyrogen test. NCL150-3 alone did not induce IL-1β secretion. However, NCL150-3 reduced the IL-1β response of LPS when combined with the positive control. NCL150 therefore has potential to inhibit the pyrogenic properties of endotoxin. The mechanism of inhibition is unknown. Several literature reports propose anti-inflammatory properties of curcumin [2-9], and preliminary NCL data discussed in the immunological section suggests that the polymer component of the formulation is immunosuppressive (Figure IV-6). The anti-pyrogenic effects observed in this assay, however, are less likely due to the curcumin since the loading of this component in NCL150-3 is very low (<1%).

II. Physicochemical Characterization

Section Summary

NCL149, the void polymer, and NCL150, the curcumin encapsulated polymer , i.e. nanocurcumin, were measured by dynamic light scattering (DLS) for hydrodynamic diameter size/size distribution and zeta potential for surface charge assessment. NCL149 had a bimodal size distribution with the major peak at ~14 nm, and a minor population 100-1000 nm (Figure II-1). NCL150 also displayed a bimodal size distribution, with peaks at ~10 nm and ~88 nm. However, the majority of the sample corresponds to the ~10 nm peak (based on the volume distribution plot). The zeta potentials for both NCL149 and NCL150 were similar, and both were negative. NCL149 had a zeta potential of -13 mV and NCL150 had a zeta potential of -17mV (Table II-2).

One batch of NCL149, and three separate batches of NCL150 were assessed. All three batches of NCL150 were in close agreement with respect to hydrodynamic diameter and zeta potential.

Hydrodynamic Size/Size Distribution via Dynamic Light Scattering (PCC-1)

Design and Methods

Dynamic light scattering (DLS) is a useful way to obtain information about the hydrodynamic size (diameter) of a nanoparticle in solution. A Malvern Zetasizer Nano ZS instrument (Southborough, MA) with back scattering detector (173°) was used for measuring the hydrodynamic size (diameter) in batch mode at 25°C in a quartz microcuvette. Samples were prepared at 4 mg/mL (NCL149-1, NCL150-1, NCL150-2) or 1 mg/mL (NCL150-3) in PBS; concentration is based on total formulation. All samples were filtered thru a 0.2 μm filter (Anotop 10 Plus, Whatman) before measurements were made.

Hydrodynamic size is reported as the intensity-weighted average and as the volume-weighted average over a particular range of size populations corresponding to the most prominent peak. The Int-Peak value is used as the hydrodynamic diameter of a particular species. The Vol-Peak and %Vol values are used to approximate relative amounts of various species in the formulation. Z-Avg values are generally used to assess batch-to-batch variability of a sample. Traces in the figures represent the average of at least twelve measurements.

Results

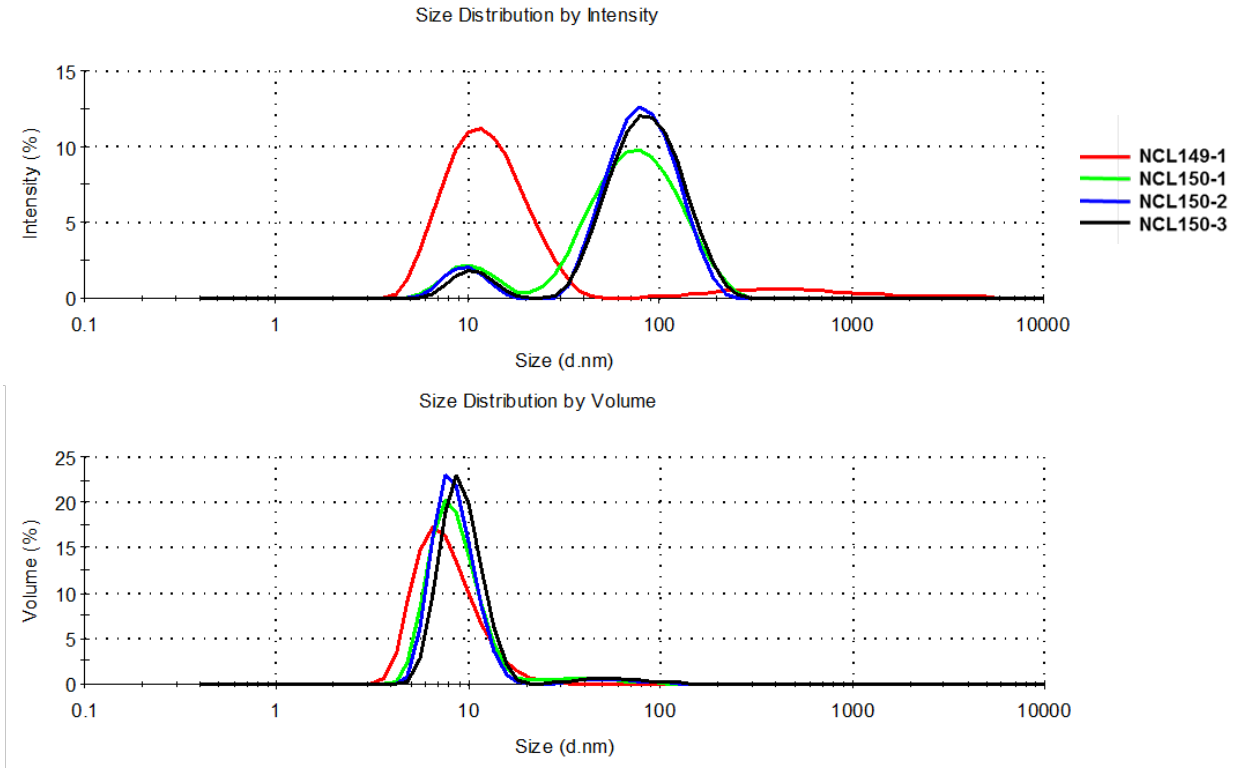

Figure II-1. The averaged intensity and volume distribution plots for NCL149 and NCL150 in PBS.

Table II-1. Summary of the hydrodynamic size data for NCL149 and NCL150 in PBS.

Sample	Z-Avg nm	PdI	Int-Peak nm	%Int	Vol-Peak nm	%Vol
NCL149-1	12.2 (0.1)	0.253 (0.008)	13.5 (0.5)	91.8 (1.7)	8.1 (0.3)	100 (0)
NCL150-1	48.7 (0.9)	0.393 (0.054)	84.9 (2.0)	88.6 (1.3)	47.7 (2.3)	3.9 (0.2)
NCL150-2	57.9 (0.7)	0.316 (0.005)	87.3 (1.4)	91.3 (0.3)	60.8 (1.3)	3.0 (0.4)
NCL150-3	62.4 (0.8)	0.304 (0.008)	92.4 (1.4)	92.4 (0.8)	62.3 (4.3)	4.2 (0.7)

Note: Results are the average of at least 12 measurements. Standard deviations are given in parentheses. Z-Avg is the intensity-weighted average. PdI is the polydispersity index. Int-Peak is the intensity-weighted average over the primary peak. % Int is the percentage of the intensity spectra occupied by the primary peak. Vol-Peak is the volume-weighted average over the primary peak. % Vol is the percentage of the volume spectra occupied by the primary peak.

Analysis and Conclusions

The hydrodynamic size (diameter) was measured using batch-mode DLS. The intensity and volume distribution plots are shown in Figure II-1 and the results summarized in Table II-1. The void polymer (NCL149-1) exhibited a bimodal size distribution with the major peak at ~14 nm, and a minor size population covering ~100-1000 nm. Incorporation of curcumin (NCL150) resulted in a bimodal size distribution with peaks centered at ~10 nm and ~88 nm. It is interesting to note that while an increased size population is observed (the ~88 nm peak), the majority of the sample (as determined by the volume distribution) corresponds to the smaller peak (~10 nm) which is similar in size than the void polymer (NCL149-1). Good batch-to-batch consistency in terms of size was observed for the multiple NCL150 lots. The size results are in agreement with the sponsor's size specification of <100 nm.

Zeta Potential (PCC-2)

Design and Methods

Zeta potential provides a measure of the electrostatic potential at the surface of the electrical double layer and the bulk medium, which is related to its surface charge. A Malvern Zetasizer Nano ZS instrument was used to measure zeta potential at 25°C for all samples. Samples were prepared at either 4 mg/mL (NCL149-1, NCL150-1, NCL150-2) or 1 mg/mL (NCL150-3) in 10 mM NaCl. Sample pH was measured before loading into a pre-rinsed folded capillary cell. An applied voltage of 150 V was used for all samples. Traces in the figures represent the average of three measurements.

The instrument was validated by running an appropriate standard (Zeta Potential Transfer Standard, DTS0050, zeta potential value of -68 ± 7 mV at 25°C, Malvern Instruments). This standard was run before all zeta potential measurements.

Results

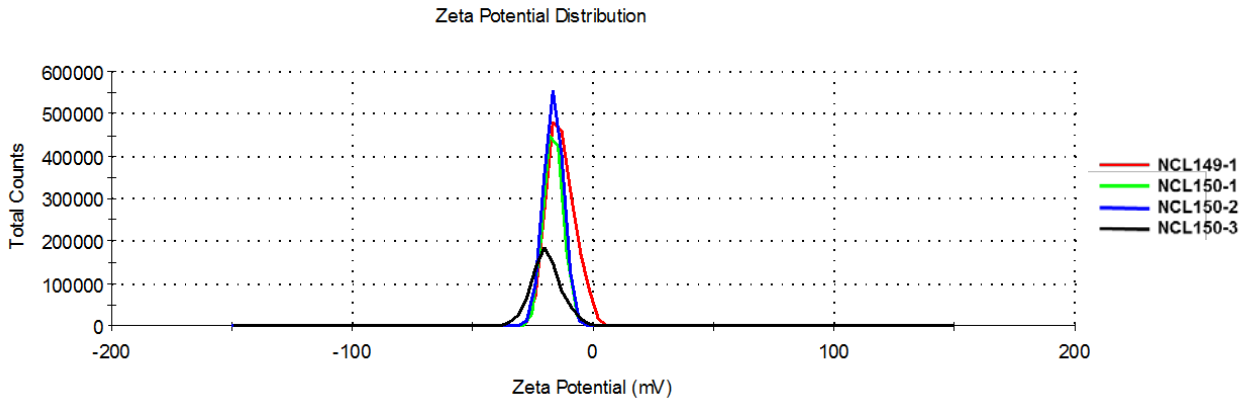

Figure II-2. The averaged zeta potential distributions for samples in 10 mM NaCl.

Table II-2. Summary of the zeta potentials for samples in 10 mM NaCl.

Sample	pH	Zeta Potential mV
NCL149-1	5.2	-13.4 (0.8)
NCL150-1	5.2	-16.3 (0.6)
NCL150-2	5.2	-16.5 (1.0)
NCL150-3	5.9	-19.3 (0.4)

Note: The standard deviations (n = 3) in each measurement are given in parentheses.

Analysis and Conclusions

The zeta potentials were measured in 10 mM NaCl and their zeta potential distributions are shown in Figure II-2. The zeta potentials and the pH for the samples are summarized in Table II-2. All samples exhibited negative zeta potentials, presumably due to the polymer in the formulation. The void polymer (NCL149-1) had the least anionic zeta potential value. Loading of drug slightly decreased the zeta potential, with batches NCL150-1 and NCL150-2 being similar. The third batch (NCL150-3) was slightly more negative relative to the previous two batches.

III. In Vitro Cytotoxicity

Section Summary

The in vitro biocompatibility of SignPath Pharma's polymeric nanoparticle with encapsulated curcumin (NCL150-3) and solvent solubilized curcumin (5% DMSO in media) were evaluated in human hepatocarcinoma (HepG2) and porcine renal proximal tubule (LLC-PK1) cell lines. Due to limited quantity, the blank polymer, NCL149, was not evaluated.

Both the HepG2 and LLC-PK1 cell lines were similarly sensitive to NCL150-3 and solvent solubilized curcumin under these assay conditions, with NCL150-3 slightly more potent than solvent solubilized curcumin. The 48 h IC_{50} value for NCL150-3, based on the MTT assay, was estimated to be 0.012 (-0.005-0.029) and 0.036 (0.026-0.045) mM [mean (95% CI)] for HepG2 and LLC-PK1 cell lines, respectively. The 48 h IC_{50} value for solvent solubilized curcumin, based on the MTT assay, was estimated to be 0.59 (0.20-0.98) and 0.25 mM (estimated from partial response), for HepG2 and LLC-PK1 cell lines, respectively.

LDH and MTT Cytotoxicity Assays in HepG2 Cells (GTA-2)

Design and Methods

The objective of this study was to evaluate the cytotoxicity of NCL150-3 and solvent solubilized curcumin (5% DMSO in media) in human hepatocarcinoma cells (HepG2).

Cytotoxicity was determined as described in NCL method GTA-2, HepG2 Human Hepatocarcinoma Cytotoxicity Assay (http://ncl.cancer.gov/working_assay-cascade.asp). Briefly, test materials were diluted to the desired assay concentrations in cell culture media (0.0000153-1 mM curcumin). Cells were plated in 96-well, microtiter plate format. Cells were preincubated for 24 h (at 5% CO_2, 37°C and 95% humidity) prior to test material addition, reaching an approximate confluence of 80%. Cells were then exposed to test material for 4, 24, and 48 h in the dark, and cytotoxicity was determined using the MTT [3-(4,5-dimethylthiazol-2-yl)-2,5-diphenyltetrazolium bromide] cell viability and lactose dehydrogenase (LDH) membrane integrity assays. In order to estimate IC_{50} values, the 48 h MTT cytotoxicity assay for complete (0-100% viability) dose-response curves were fit to the Michaelis Menten equation,

$$E = E_{max} * C^{\gamma} / (C^{\gamma} + IC_{50}^{\gamma})$$

using nonlinear regression analysis (WinNonlin, Pharsight Corp., Mountain View, CA).

where E: Effect
- E_{max}: Maximal effect (~100% cell death)
- C: drug concentration
- γ: Sigmoidicity constant
- IC_{50}: Inhibitory concentration 50%

Results

The maximum concentration of nanoparticle tested in the HepG2 cytotoxicity study was 1 mM curcumin. In HepG2 cells, treatment of cells with NCL150-3 resulted in a loss of cell viability (Figure III-1A), as determined by MTT assay. A corresponding loss of membrane integrity, as determined by the LDH leakage assay (Figure III-1B), was also observed. The LDH leakage dose-response was incomplete and not of the magnitude of the MTT response, with a maximal plateau of approximately 92% loss of membrane integrity. Solvent solubilized curcumin was less toxic than NCL150-3 under these assay conditions (Figure III-2). The 48 h IC_{50} value for NCL150-3 and solvent solubilized curcumin, based on MTT assay, was estimated to be 0.012 (-0.005-0.029) mM and 0.59 (0.20-0.98) mM [mean (95% CI)], respectively.

The LDH assay can be prone to artifacts, most likely due to effects from the formulation. This is evident especially in Figure III-1B. The 48 hr LDH trace does not correlate with the 48 hr MTT trace. Therefore, this data should not be used for comparison to the solvent solubilized curcumin. All comparisons were made using the MTT data.

A. MTT Assay

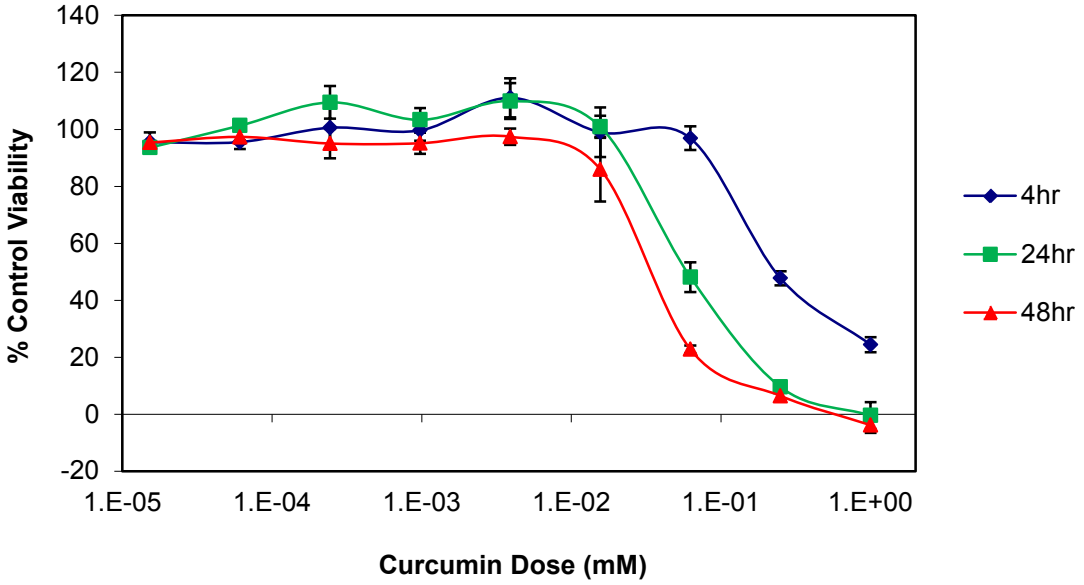

B. LDH Assay

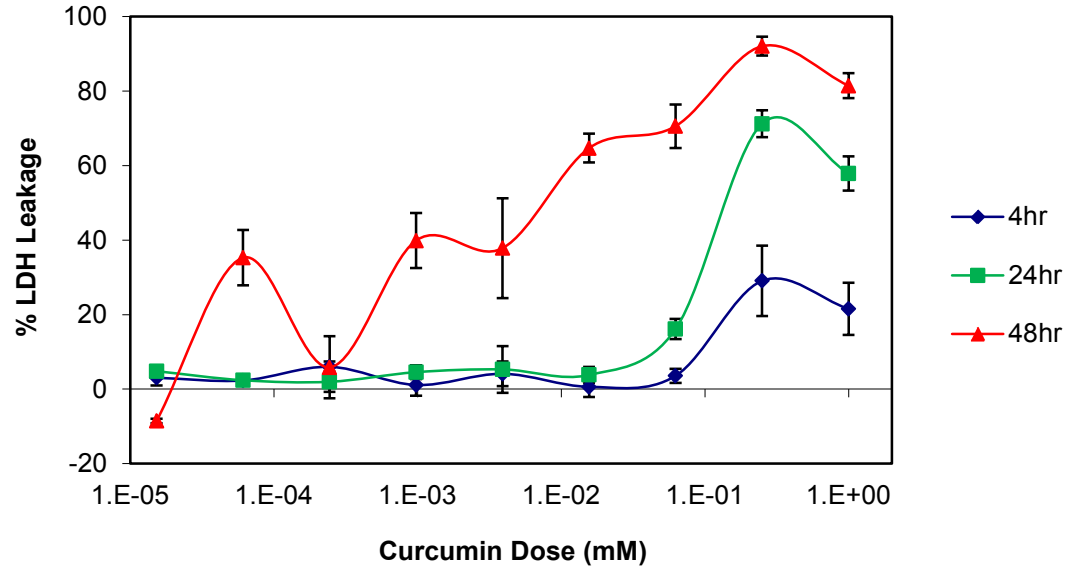

Figure III-1. NCL150-3 cytotoxicity assay in HepG2 cells. Human hepatocarcinoma cells were treated for 4, 24, and 48 h with NCL150-3 (0.0000153-1 mM curcumin). Cytotoxicity was determined at each time point by the **(A)** MTT or **(B)** LDH assays, as described in the Hep G2 Hepatocarcinoma Cytotoxicity Assay (GTA-2). Data represents the mean ± SE, *N*=3.

A. MTT Assay

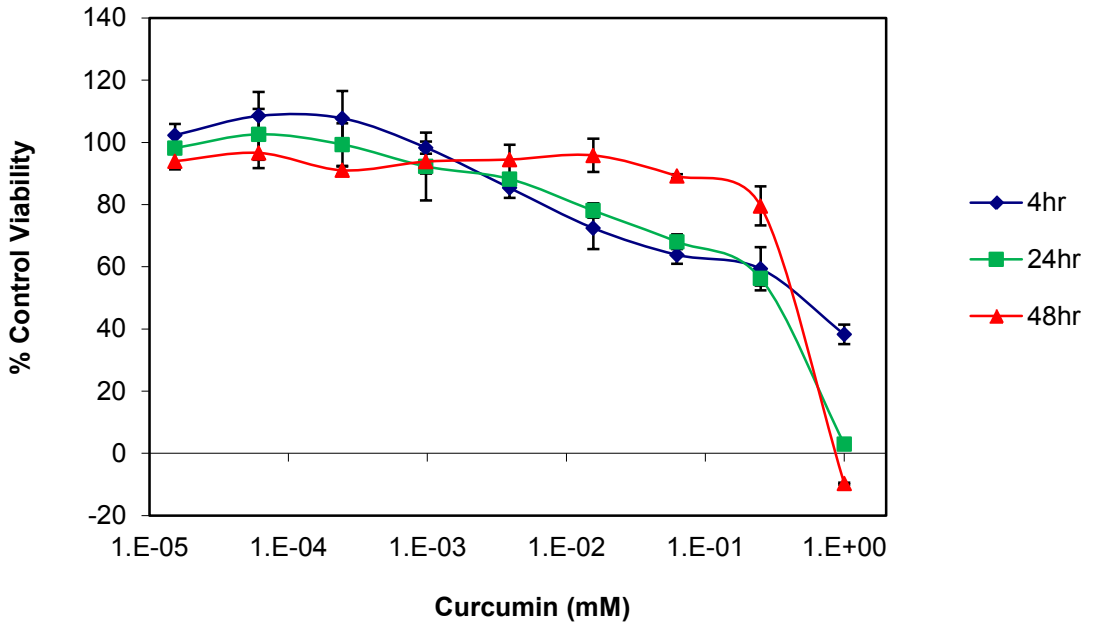

B. LDH Assay

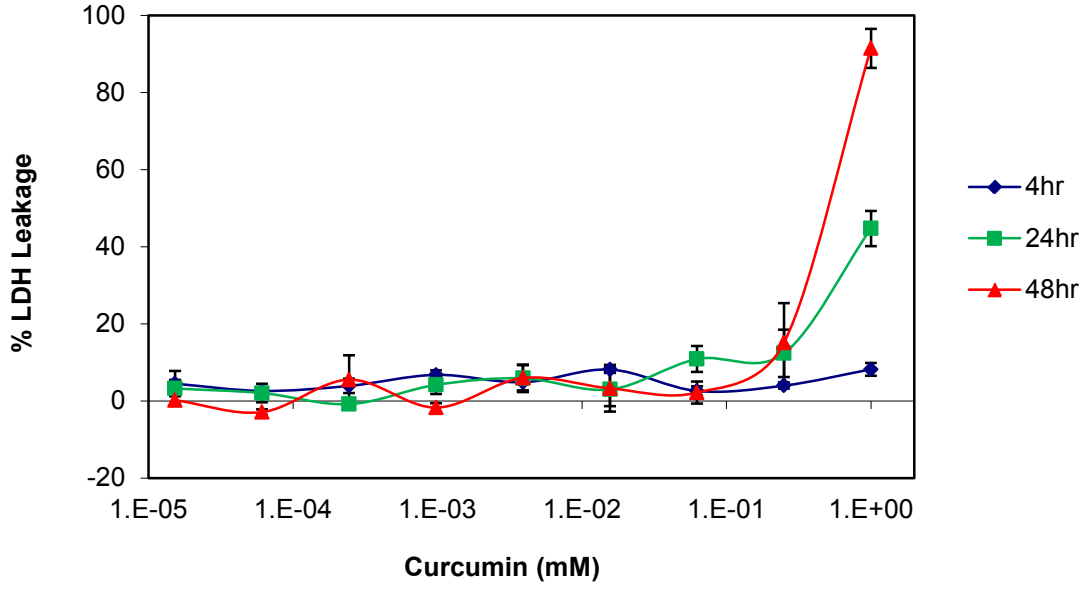

Figure III-2. Solvent solubilized curcumin cytotoxicity assay in HepG2 cells. Human hepatocarcinoma cells were treated for 4, 24, and 48 h with 0.0000153-1 mM curcumin (5% DMSO in media). Cytotoxicity was determined at each time point by the **(A)** MTT or **(B)** LDH assays, as described in the HepG2 Hepatocarcinoma Cytotoxicity Assay (GTA-2). Data represents the mean ± SE, *N*=3.

Analysis & Conclusion

NCL150-3 and solvent solubilized curcumin were minimally toxic to HepG2 cells, with treatment resulting in loss of cell viability and membrane integrity only at the highest concentrations tested, in the high micromolar-millimolar range.

LDH and MTT Cytotoxicity Assays in LLC-PK1 Cells (GTA-1)

Design and Methods

The objective of this study was to evaluate the cytotoxicity of NCL150-3 and solvent solubilized curcumin (5% DMSO in media) in porcine renal proximal tubule (LLC-PK1) cells.

Cytotoxicity was determined as described in NCL method GTA-1, LLC-PK1 Kidney Cytotoxicity Assay (http://ncl.cancer.gov/working_assay-cascade.asp). Briefly, test materials were diluted to the desired assay concentrations in cell culture media (0.0000153-1 mM curcumin). Cells were plated in 96-well, microtiter plate format. Cells were preincubated for 24 h prior to test material addition, reaching an approximate confluence of 80%. Cells were then exposed to test material for 4, 24, and 48 h in the dark, and cytotoxicity was determined using the MTT cell viability and LDH membrane integrity assays. In order to estimate IC_{50} values, the 48 h MTT cytotoxicity assay for complete (0-100% viability) dose-response curves were fit to the Michaelis Menten equation,

$$E = E_{max} * C \, (C + IC_{50})$$

using nonlinear regression analysis (WinNonlin, Pharsight Corp., Mountain View, CA). The 48 h IC_{50} for partial dose-response profiles were estimated directly from data.

Results

The maximum concentration of nanoparticle tested in the LLC-PK1 cytotoxicity study was 1 mM curcumin. In LLC-PK1 cells, treatment of cells with NCL150-3, resulted in a loss of cell viability (Figure III-3A), as determined by the MTT assay. A corresponding loss of membrane integrity, as determined by the LDH leakage assay (Figure III-3B), was also observed. The LDH leakage dose-response was incomplete and not of the magnitude of the MTT response, with a maximal plateau of approximately 45% loss of membrane integrity. The solvent solubilized curcumin was less toxic than NCL150-3 under these assay conditions (Figure III-4), and resulted in only a partial dose response. The 48 h IC_{50} value for NCL150-3 and solvent solubilized curcumin, based on the MTT assay, was estimated to be 0.036 (0.026-0.045) mM and 0.25 mM (estimated from partial response) [mean (95% CI)], respectively.

A. MTT Assay

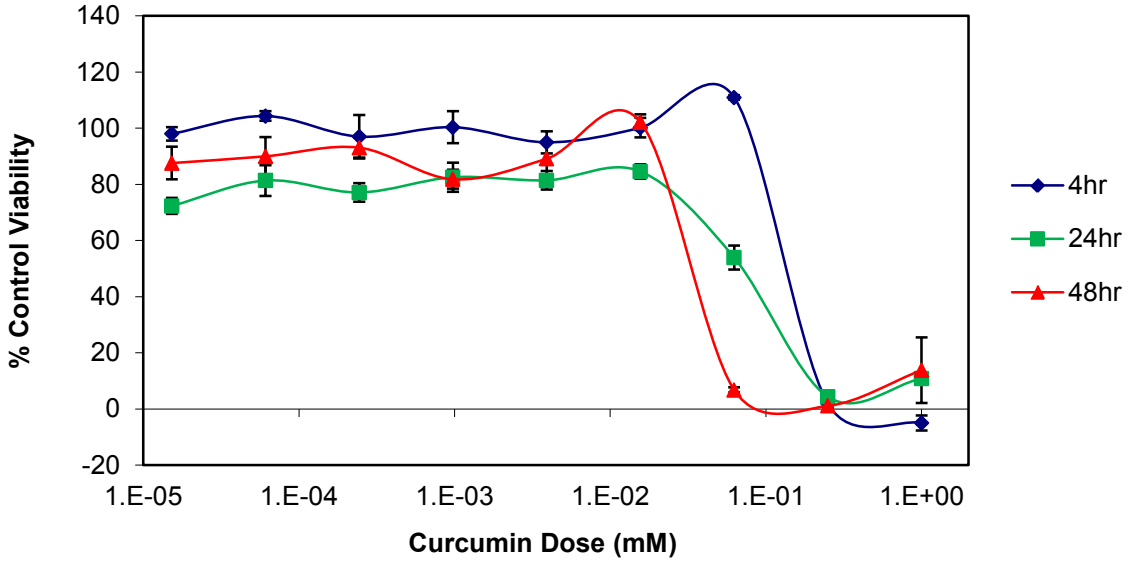

B. LDH Assay

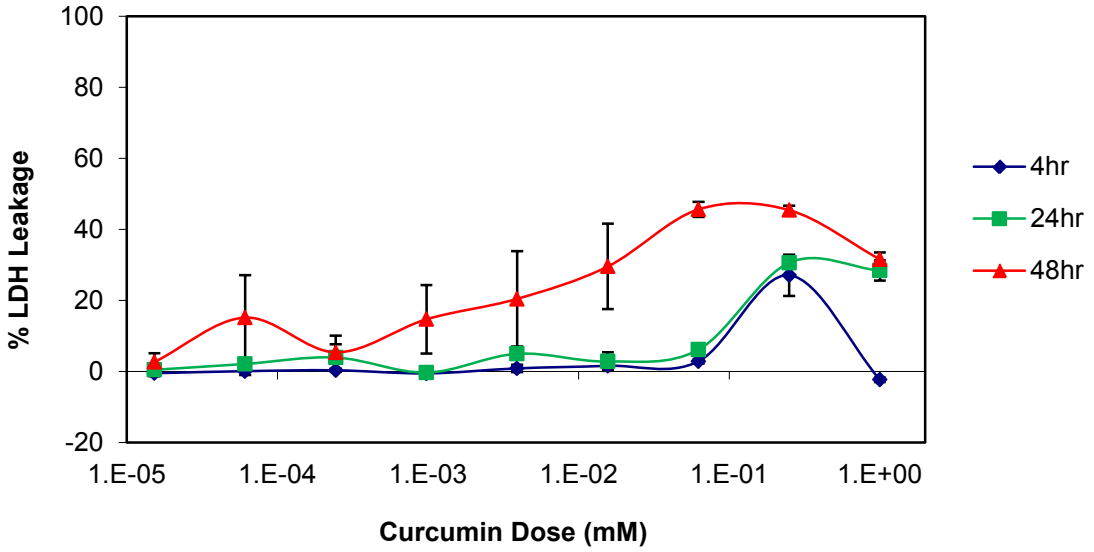

Figure III-3. NCL150-3 cytotoxicity assay in LLC-PK1 cells. Kidney cells were treated for 4, 24, and 48 h with NCL150-3 (0 0000153-1 mM curcumin). Cytotoxicity was determined at each time point by the **(A)** MTT or **(B)** LDH assays, as described in the LLC-PK1 Kidney Cytotoxicity Assay (GTA-1). Data represents the mean ± SE, *N*=3.

A. MTT Assay

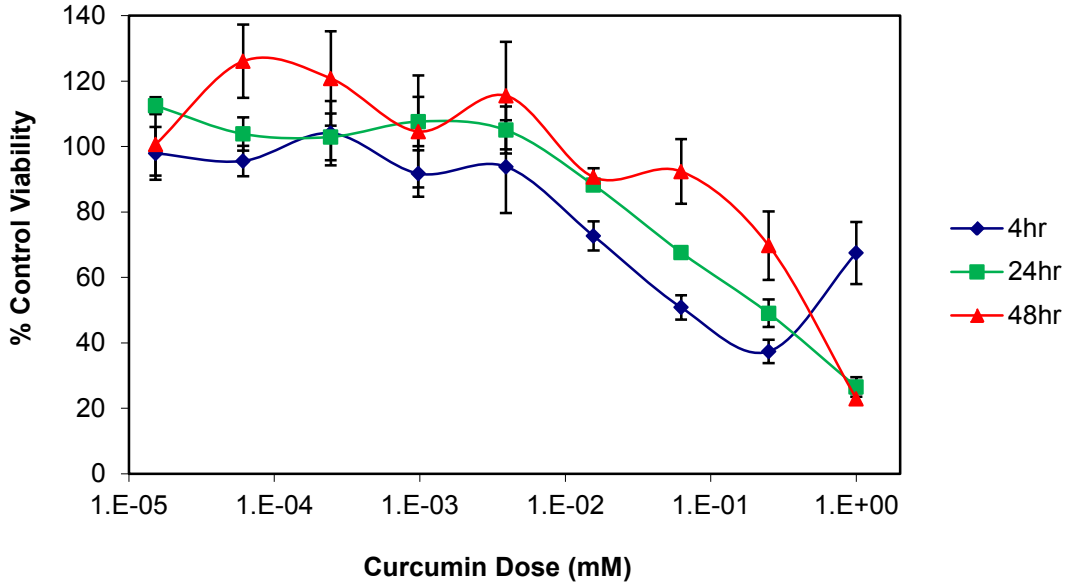

B. LDH Assay

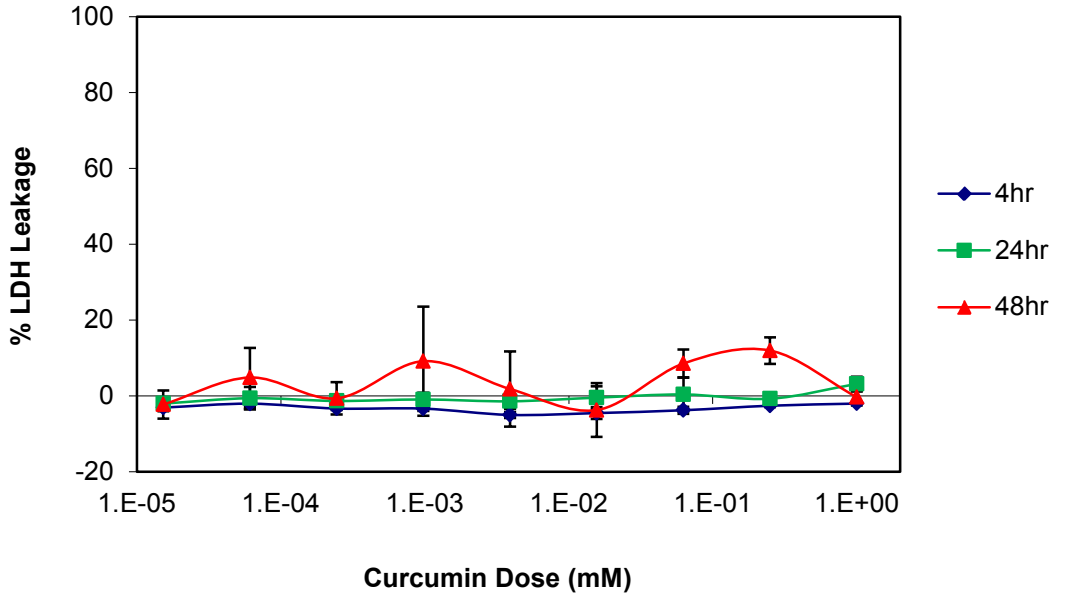

Figure III-4. Solvent solubilized curcumin cytotoxicity assay in LLC-PK1 cells. Kidney cells were treated for 4, 24, and 48 h with 0 0000153-1 mM curcumin (5% DMSO in media). Cytotoxicity was determined at each time point by the **(A)** MTT or **(B)** LDH assays, as described in the LLC-PK1 Kidney Cytotoxicity Assay (GTA-1). Data represents the mean ± SE, *N*=3.

Table III-1. 48 h IC_{50} values, based on MTT assay data.

Treatment	LLC-PK1 mean (95%CI) mM	Hep G2 mean (95%CI) mM
NCL150-3	0.036 (0.026-0.045)	0.012 (-0.005-0.029)
Solvent-solubilized Curcumin	0.25[a]	0.59 (0.20-0.98)

[a] IC_{50} for partial dose response estimated from the graph.

Analysis and Conclusion

NCL150-3 and solvent solubilized curcumin were minimally toxic, with treatment resulting in loss of cell viability and membrane integrity only at the highest concentrations tested, in the high micromolar-millimolar range.

IV. In Vitro Immunological Characterization

Section Summary

The purpose of this study was test the hematocompatibility and effects on immune cell functions of the polymeric formulation of curcumin, NCL150. The void polymer formulation, NCL149, was used as a control in some experiments; due to its' limited supply, NCL149 was not used in all assays. NCL149 was only used in assays where positive responses with NCL150 were observed.

NCL150-3 was assessed for hemolytic properties, ability to induce platelet aggregation, effects of coagulation time, and ability to active the human complement system. The nanocurcumin formulation, at the tested concentrations, was not hemolytic (Figure IV-1), did not induce platelet aggregation in vitro (Figure IV-2A), did not interfere with coagulation times as measured by prothrombin time, activated partial thromboplastin time or thrombin time (Figure IV-3), and did not activate the complement system in vitro (Figure IV-4). When tested at the highest concentration only (21 mg/mL), NCL150-3 did suppress collagen-induced platelet aggregation (Figure IV-2B).

In addition to the above noted hematocompatibility assays, NCL150-3 was also assessed for effects on leukocyte proliferation, ability to induce nitric oxide production, and effects on chemotaxis. The nanocurcumin formulation, at the tested concentrations, did not induce leukocyte proliferation (Figure IV-5A), did not induce oxidative burst in macrophages (Figure IV-7), and did not induce chemotaxis (Figure IV-8). When tested at the two highest concentrations only (2.1 and 21 mg/mL), NCL150-3 did suppress PHA-M induced leukocyte proliferation (Figure IV-5B).

Finally, NCL150-3 was assessed for effects on cytokine secretion by PBMC and for effects of the cytotoxicity of NK cells. The nanocurcumin formulation showed considerable induction of IL-8 and low-level induction of TNFα (Table IV-1). In addition, the nanoformulation showed suppression of LPS-induced expression of the pyrogenic cytokines TNFα and IL-1β. At the two highest concentrations tested (2.1 and 21 mg/mL), NCL150-3 inhibited the cytotoxicity of NK cells (Figure IV-9). These data suggest NCL150 has immunosuppressive properties.

Concentration Selection

All concentrations discussed in this section reflect the total formulation, which includes curcumin formulated into the polymeric carrier. Since curcumin loading was less than 1%, preparing samples for in vitro studies using curcumin concentrations was not feasible due to the high viscosity associated with high concentrations of the polymeric component of the formulation.

For in vitro immunological analyses, NCL150-3 was tested at four concentrations: 0.021, 0.21, 2.1 and 21.0 mg/mL, of which 0.021 mg/mL is the theoretical blood concentration in human blood when this formulation is used at the sponsor's estimated therapeutic dose.

To calculate this concentration, we first converted the efficacious mouse dose to a human dose:

25 mg/kg ÷ 12 = 2.08 mg/kg

Then we assumed that an average patient's weight is 70 kg, with a blood volume of 7000 mL (10% of body weight), and that all injected material will stay in circulation:

2.08 mg/kg x 70 kg = 145.8 mg in 7000 mL of blood or 0.021 mg/mL

(Factors 12 vs. of 12.3 and blood volume of 10% instead of 8 or 9% were used for simpler mathematical calculation.)

Nanoparticle Hemolytic Properties (ITA-1)

Design and Methods

The objective of this experiment was to evaluate the nanoparticle's effect on the integrity of human red blood cells in vitro following NCL protocol ITA-1, Analysis of Hemolytic Properties of Nanoparticles (http://ncl.cancer.gov/working_assay-cascade.asp). NCL150-3 was tested at 4 concentrations: 0.021, 0.21, 2.1 and 21.0 mg/mL of nanocurcumin.

Results

No detectable hemolysis was observed at any of the tested concentrations under the experimental conditions utilized (Figure IV-1).

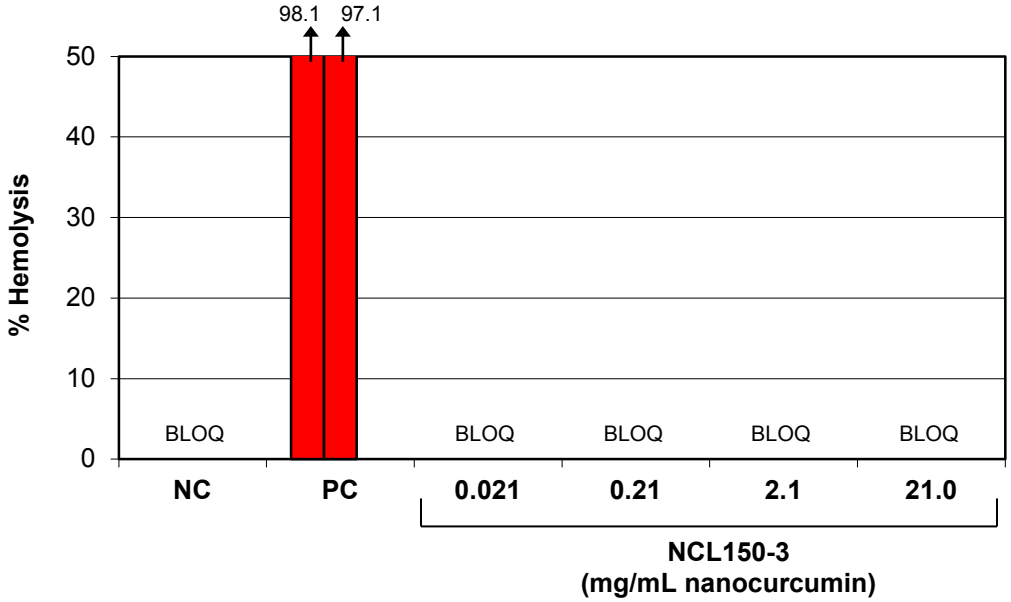

Figure IV-1. Analysis of nanoparticle hemolytic properties (ITA-1). NCL150-3 was used to evaluate potential particle effects on the integrity of red blood cells. Three independent samples were prepared for each nanoparticle concentration and analyzed in duplicate (%CV < 20). Each bar represents the mean of triplicate results. Triton X-100 was used as a positive control (PC). PBS was used to reconstitute nanoparticles and represented the negative control (NC).

Analysis and Conclusions

NCL150-3 did not disturb the integrity of human red blood cells *in vitro* under the tested conditions.

Nanoparticle Ability to Induce Platelet Aggregation (ITA-2)

Design and Methods

The objective of this experiment was to evaluate the effect of nanoparticles on human platelets *in vitro* following NCL protocol ITA-2, Analysis of Platelet Aggregation (http://ncl.cancer.gov/working_assay-cascade.asp). NCL150-3 was tested at 4 concentrations: 0.021, 0.21, 2.1 and 21.0 mg/mL of nanocurcumin.

Results

No platelet aggregation (Figure IV-2A) and no change in collagen-induced platelet aggregation (Figure IV-2B) were detected in vitro when NCL150-3 was tested at concentrations ranging from 0.021 to 2.1 mg/kg. At the highest tested concentration (21 mg/kg), however, weak platelet aggregation and suppression of collagen-induced platelet aggregation were observed (Figures IV-2A and IV-2B, respectively).

A. Nanoparticles

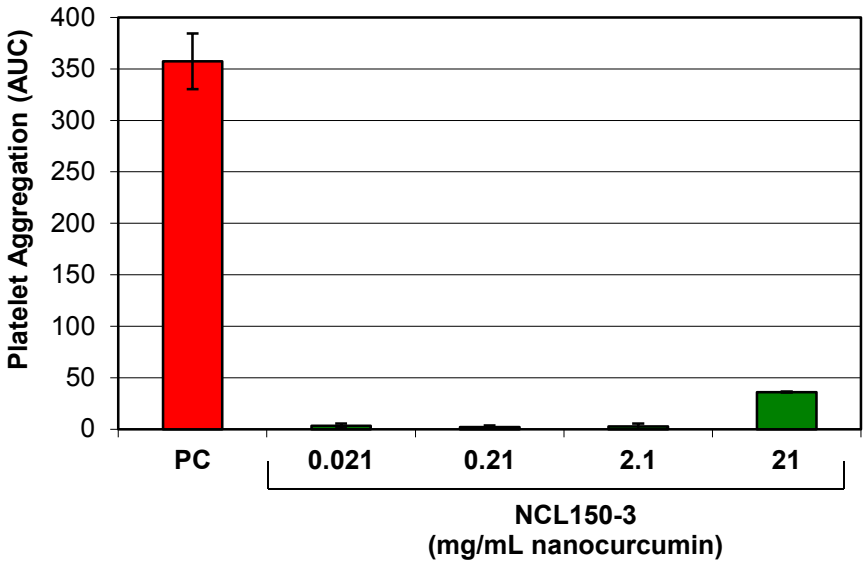

B. Nanoparticles + Collagen

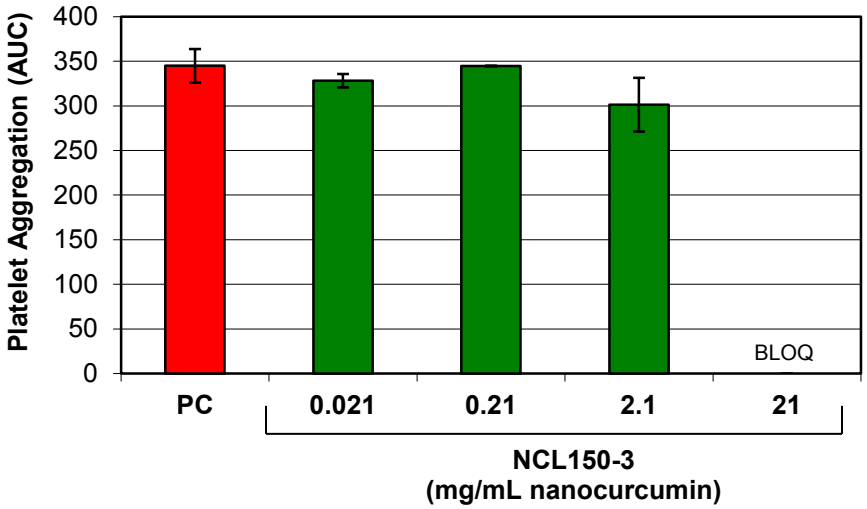

Figure IV-2. Analysis of nanoparticle ability to induce platelet aggregation (ITA-2). (A) NCL150-3 was used to evaluate potential particle effects on the cellular component of the blood coagulation cascade. For each nanoparticle concentration, three independent samples were prepared and analyzed in duplicate (%CV < 20). Each bar represents the mean of triplicate results. Positive control (PC) was collagen. **(B)** Collagen treatment was combined with nanoparticles. For each nanoparticle concentration, three independent samples were prepared and analyzed in duplicate (%CV < 20). Each bar represents the mean of triplicate results.

Analysis and Conclusions

NCL150-3 was not thrombogenic in vitro and did not interfere with collagen-induced platelet aggregation at concentrations ranging 0.021 to 2.1 mg/mL. At 21 mg/mL, however, NCL150-3 induced weak platelet aggregation and suppressed collagen-induced platelet aggregation. The mechanism of the observed inhibition is unknown.

Nanoparticle Effect on Coagulation (ITA-12)

Design and Methods

The objective of this experiment was to evaluate the effect of nanoparticle treatment on human plasma coagulation *in vitro* following NCL protocol ITA-12, Coagulation Assay (http://ncl.cancer.gov/working_assay-cascade.asp). NCL150-3 was tested at 4 concentrations: 0.021, 0.21, 2.1 and 21.0 mg/mL of nanocurcumin.

Results

No physiologically significant change in plasma coagulation was observed in prothrombin time (PT), activated partial thromboplastin time (APTT) and thrombin time assays. A statistically significant prolongation of coagulation time was detected at the highest tested concentration (Figure IV-3) for all three assays.

A. Prothrombin Time

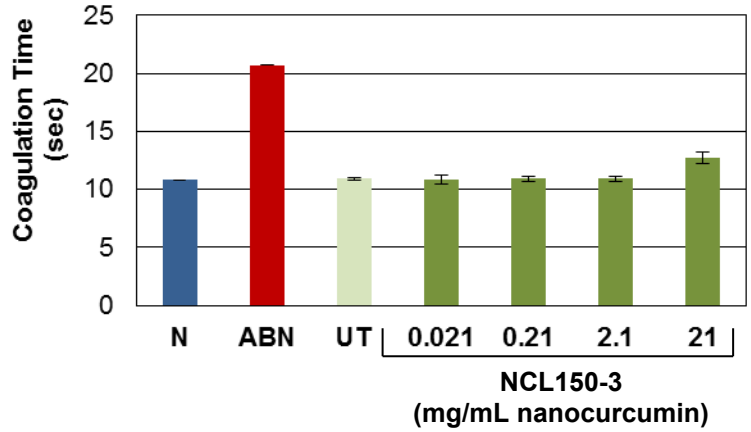

B. Activated Partial Thromboplastin Time

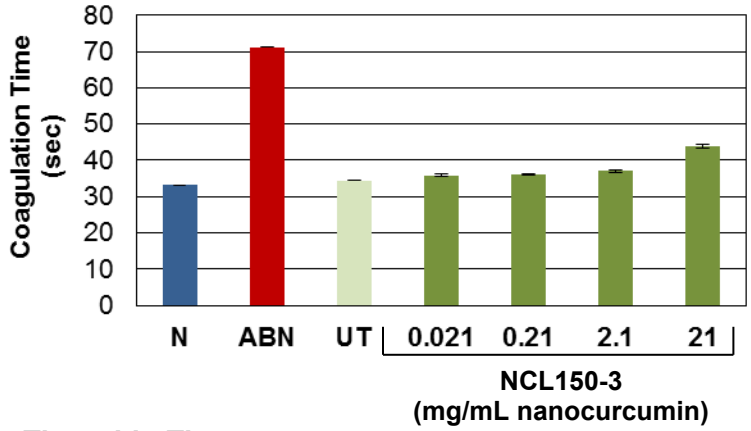

C. Thrombin Time

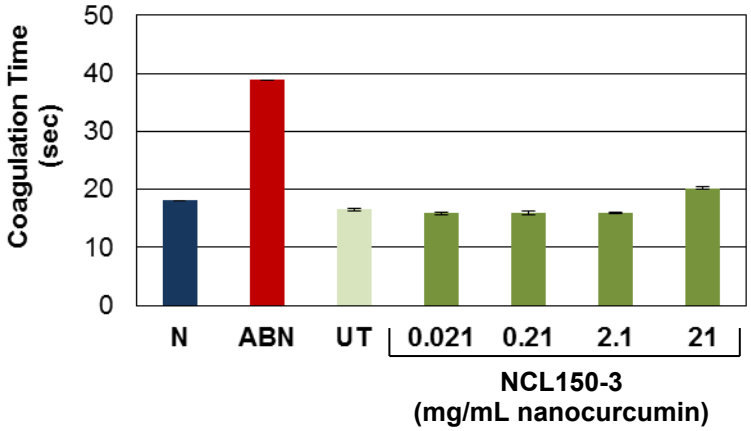

Figure IV-3. Analysis of nanoparticle effects on coagulation (ITA-12). NCL150-3 was tested *in vitro* to evaluate potential particle effects on the biochemical component of the blood coagulation cascade. For each nanoparticle, three independent samples were prepared and analyzed in duplicate (%CV < 5). Each bar represents the mean of triplicate results. Normal plasma standard (N) and abnormal plasma standard (ABN) were used for instrument controls. Plasma pooled from at least three donors was either untreated (UT) or treated with NCL150-3 at four concentrations.

Analysis and Conclusions

NCL150-3 did not interfere with plasma coagulation *in vitro*. Only a slight prolongation of coagulation time was seen for the highest tested concentration. However, since the observed prolongation was less than 2-fold, it is not likely to be physiologically relevant. Furthermore, this could be attributed to in vitro artifacts when this formulation is tested at very high concentrations.

Complement Activation (ITA-5.2)

Design and Methods

The objective of this experiment was to evaluate the effect of nanoparticles on the human complement system. For quantitative evaluation of complement activation, samples were prepared according to the procedure described in ITA-5.2, Quantitative Analysis of Complement Activation (http://ncl.cancer.gov/working_assay-cascade.asp). NCL150-3 was tested at three concentrations: 0.21, 2.1 and 21.0 mg/mL of nanocurcumin.

Results

NCL150-3 did not induce significant complement activation in vitro under the tested assay conditions at any of the three tested concentrations (Figure IV-4).

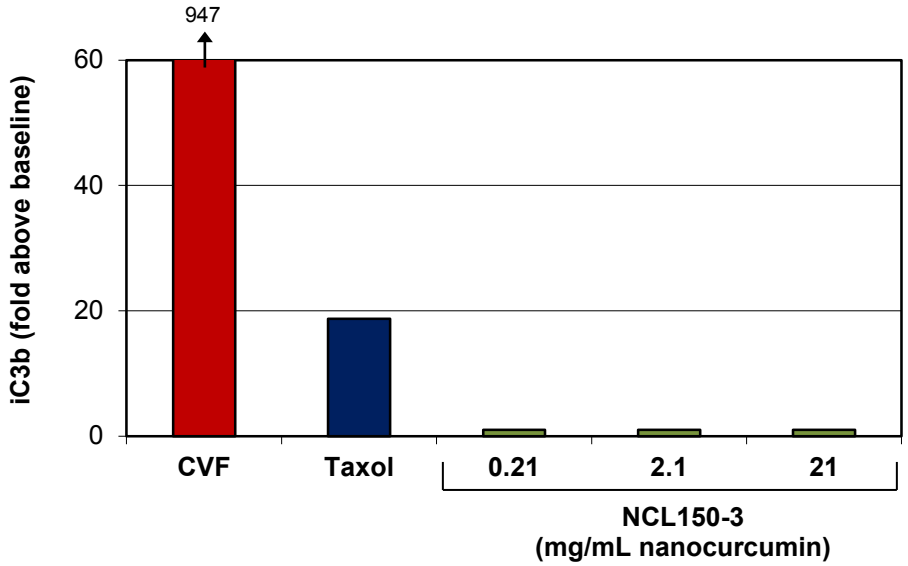

Figure IV-4. *In vitro* analysis of complement activation (ITA-5.2). NCL150-3 was tested for the ability to activate the human complement system. PBS and cobra venom factor (CVF) were used as the negative and positive control, respectively. Taxol was used as an additional, clinically relevant positive control. Three independent samples were prepared for each formulation and analyzed in duplicate (%CV <20). Shown is the mean of triplicate results. Data is presented as fold induction over negative control.

Analysis and Conclusions

NCL150-3 did not induce complement activation *in vitro* under the experimental conditions.

Nanoparticle Effect on Leukocyte Proliferation (ITA-6)

Design and Methods

The objective of this experiment was to evaluate the effect of nanoparticle treatment on the proliferation of human leukocytes *in vitro* following NCL protocol ITA-6, Leukocyte Proliferation Assay (http://ncl.cancer.gov/working_assay-cascade.asp). NCL150-3 was tested at four concentrations: 0.021, 0.21, 2.1 and 21.0 mg/mL of nanocurcumin.

Results

NCL150-3 did not induce leukocyte proliferation at any of the tested concentrations (Figure IV-5A). At 2.1 and 21.0 mg/mL concentrations NCL150-3 suppressed PHA-M induced proliferation (Figure IV-5B).

A. Nanoparticles

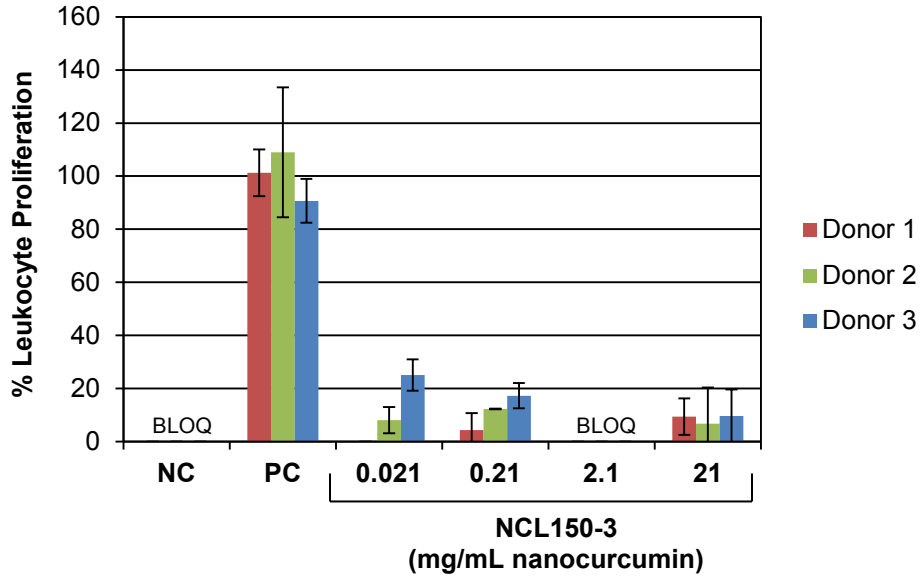

B. Nanoparticles + PHA-M

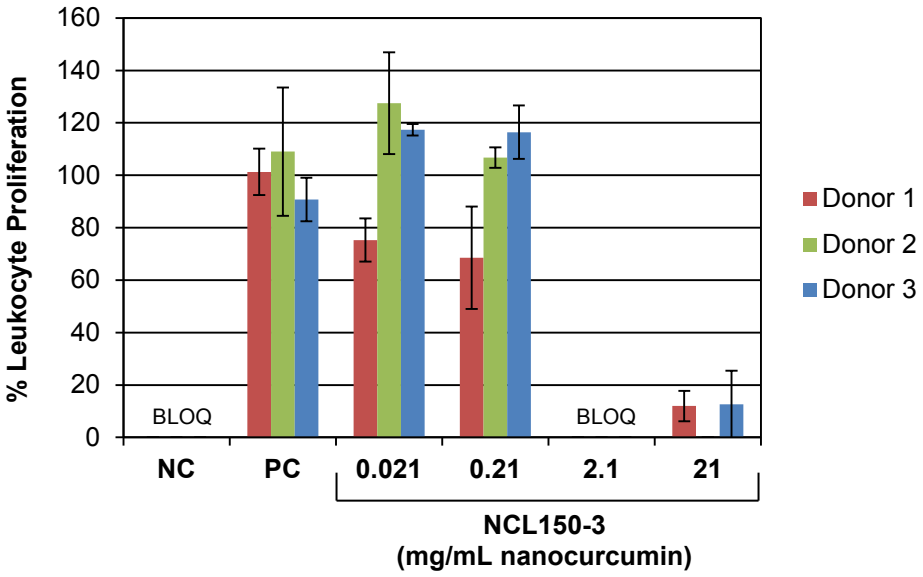

Figure IV-5. Analysis of nanoparticle effects on leukocyte proliferation (ITA-6). NCL150-3 was tested for **(A)** the ability to induce leukocyte proliferation and **(B)** to inhibit mitogen-mediated leukocyte proliferation. Phytohemaglutinin-M (PHA-M) was used as a positive control (PC) for proliferation induction. For each nanoparticle concentration, three independent samples were prepared and analyzed in duplicate (%CV < 25) from three separate donors. Each bar represents the mean of triplicate results. PBS was used as a negative control (NC). **(A)** Analysis of proliferation in the presence of nanoparticle formulations. **(B)** Combination of PHA-M and nanoparticle treatments to assess potential interference with PHA-M induced proliferation.

Analysis and Conclusions

NCL150-3 did not induce leukocyte proliferation at any of the tested concentrations. At the two high concentrations, NCL150-3 suppressed PHA-M induced proliferation; this suggests NCL150-3 is immunosuppressive. PHA-M is a plant lectin and is known for its mitogen properties. PHA-M-induced leukocyte proliferation does not require presence of memory T cells and is a part of innate immunity.

Human Leukocyte Activation (HuLa) Assay (ITA-18)

Design and Methods

The objective of this experiment was to evaluate the effect of nanoparticle treatment on the proliferation of human leukocytes *in vitro* following NCL protocol ITA-18, Human Leukocyte Activation Assay. In this assay, anoparticles are tested for their ability to inhibit leukocyte proliferation in response to the flu antigen. NCL150-3 was tested at three concentrations: 0.21, 2.1 and 21.0 mg/mL of nanocurcumin. Due to limited quantities, NCL149-1 was tested at one concentration, the equivalent 2.1mg/mL of nanocurcumin. The FluZone flu vaccine formulated for the 2011-2012 season was used as the source of flu antigen. The three donors utilized in this assay received the current year flu vaccine, and an in vitro response of their leukocytes to the flu antigen was verified in preliminary experiments prior to nanoparticle testing.

Results

At all tested concentrations NCL150-3 and NCL149 suppressed flu-antigen induced proliferation (Figure III-6).

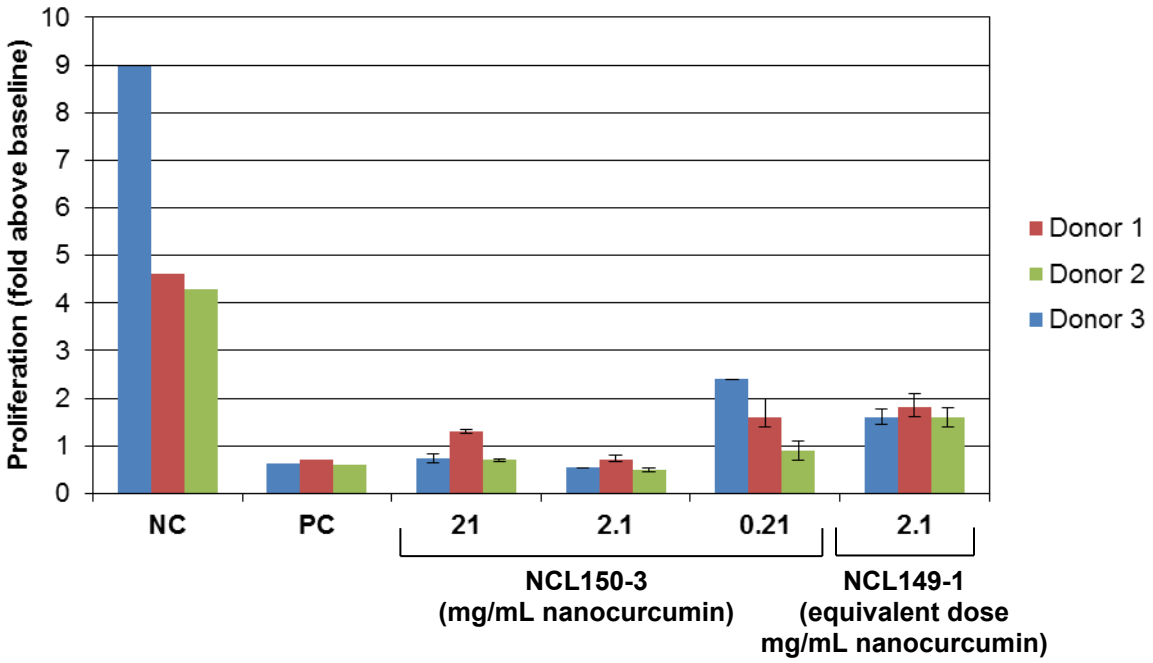

Figure IV-6. Analysis of nanoparticle effects on leukocyte proliferation (ITA-6). NCL150-3 and NCL149-1 were tested for their ability to inhibit leukocyte proliferation in response to the flu antigen. For each nanoparticle concentration, three independent samples were prepared and analyzed in duplicate (%CV < 25). Each bar represents the mean of triplicate results. PBS was used as a negative control (NC) and dexamethasone was used as the positive control (PC).

Analysis and Conclusions

NCL150-3, at all tested concentrations, suppressed flu-antigen induced proliferation. This data is in agreement with the in vitro macrophage activation test (Figure I-1) and the leukocyte proliferation assay (Figure IV-5), and suggests that NCL150-3 is immunosuppressive. Flu antigen-induced leukocyte proliferation requires the presence of memory T cells and is a part of the adaptive immunity.

Nitric Oxide Production by Macrophages (ITA-7)

Design and Methods

The objective of this experiment was to evaluate the effect of nanoparticle treatment on oxidative burst of macrophages *in vitro* following NCL protocol ITA-7, Detection of Nitric Oxide Production by RAW 264.7 Macrophage Cell Line (http://ncl.cancer.gov/working_assay-cascade.asp). NCL150-3 was tested at 4 concentrations:0.021, 0.21, 2.1 and 21.0 mg/mL of nanocurcumin.

Results

NCL150-3 at all tested concentrations did not result in induction of nitric oxide in macrophages *in vitro* (Figure IV-7).

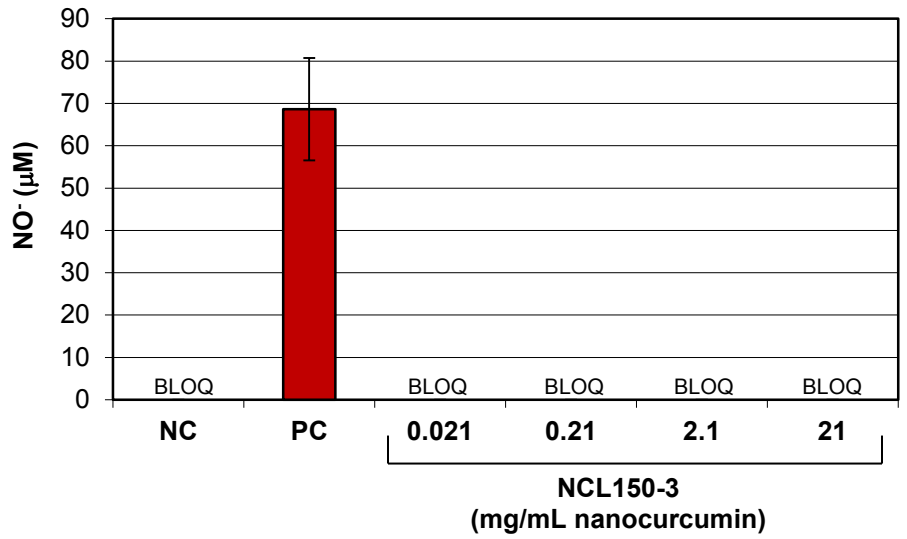

Figure IV-7. Analysis of nitric oxide (NO^-) production by macrophages (ITA-7). NCL150-3 was tested in vitro for the ability to induce nitric oxide secretion in the macrophage cell line RAW264.7. For each concentration, three independent samples were prepared and analyzed in duplicate (%CV < 25).

Analysis and Conclusions

NCL150-3 did not induce oxidative burst (NO^- induction) in macrophages under the tested *in vitro* conditions.

Nanoparticle Effect on Chemotaxis (ITA-8)

Design and Methods

The objective of this experiment was to evaluate nanoparticle effects on chemotactic mobility of macrophages following NCL protocol ITA-8, Chemotaxis Assay (http://ncl.cancer.gov/working_assay-cascade.asp). NCL150-3 was tested at four concentrations: 0.021, 0.21, 2.1 and 21.0 mg/mL of nanocurcumin.

Results

NCL150-3 did not induce chemotaxis of the macrophage-like cell line HL-60 (Figure IV-8).

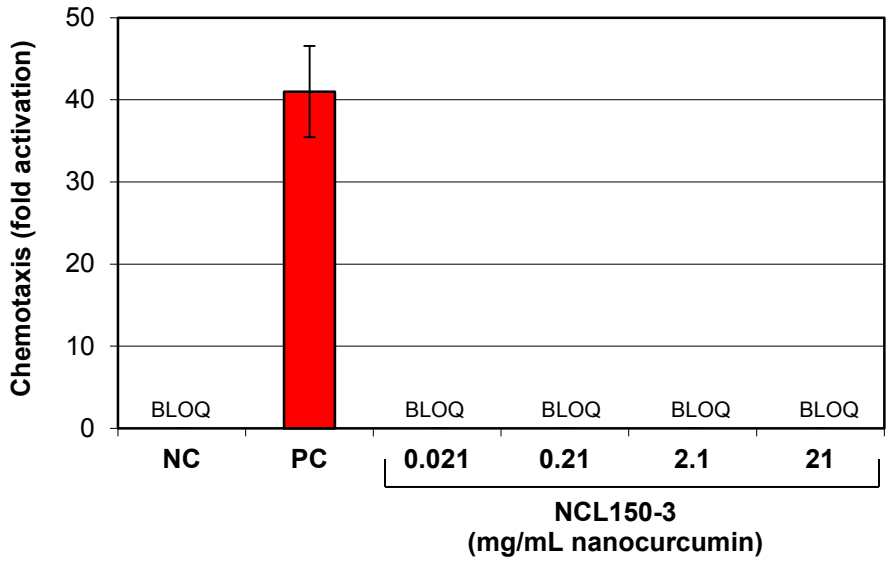

Figure IV-8. Analysis of nanoparticle effects on chemotaxis (ITA-8). NCL150-3 was tested in vitro for the ability to induce chemotaxis of HL-60 macrophage-like cells. PBS and FBS were used as negative and positive controls, respectively. Three independent samples were prepared for each formulation and tested in triplicate (%CV < 25). Shown is the mean triplicate response for each sample.

Analysis and Conclusions

NCL150-3 did not induce macrophage chemotaxis *in vitro* under the tested conditions.

Potential Effects on Cytokine Secretion by PBMC (ITA-10)

Design and Methods

The objective of this experiment was to evaluate the nanoparticles' ability to induce production of inflammatory cytokines *in vitro*. The experiment was conducted in whole blood culture. Blood was collected from three healthy human donor volunteers into Li-heparin vacutainers. The blood was diluted with negative control, positive control, or nanoparticles in PBS to a final ratio 1:5 (v:v), and cultured for 24 h at 37°C. The supernatants were analyzed for the presence of cytokines using the MSD Th1/Th2 human inflammation multiplex panel. K12 E.coli LPS at a concentration of 1 ng/mL and PHA-M at a concentration of 1 μg/mL were used as positive controls. PBS was used as the negative control, and all controls and nanoparticles were diluted into PBS. NCL150-3 was tested at four concentrations: 0.021, 0.21, 2.1 and 21.0 mg/mL of nanocurcumin.

Results

NCL150-3 resulted in robust induction of IL-8, which was enhanced by combination with positive control LPS. At 2.1 mg/mL NCL150-3 resulted in weak induction of TNFα, however TNFα, IL-1β and IFNγ induced by the positive control LPS were suppressed in the presence of NCL150-3 The data was consistent between all three donors (Table IV-1).

Table IV-1. Cytokine secretion in whole blood cultures (ITA-10). Whole blood from healthy donors were either untreated or treated for 24 h with 10 ng/mL bacterial lipopolysaccharide (PC1), 1 μg/mL PHA-M (PC2), NCL150-3 at four concentrations or a combination of NCL150-3 and lipopolysacharide. Shown is the mean of duplicate responses from one donor (CV<25%). Similar data were observed with two other donors.

Sample ID	IFN-γ (pg/mL)	IL-1 β (pg/mL)	IL-2 (pg/mL)	IL-4 (pg/mL)	IL-5 (pg/mL)	IL-8 (pg/mL)	IL-10 (pg/mL)	IL-12p70 (pg/mL)	IL-13 (pg/mL)	TNF α (pg/mL)
NC	3.3	0.0	16.3	18.2	5.8	25.0	16.8	10.6	9.8	10.2
LPS, PC1	343.8	1942.8	24.2	10.8	11.4	1512.4	26.4	15.7	46.8	1470.2
PHA-M, PC2	6759.1	734.9	228.0	21.9	7.5	2695.5	79.5	15.1	68.3	2055.6
21 mg/mL	0.0	BLOQ	14.7	0.4	BLOQ	339.2	7.5	4.5	9.2	BLOQ
2.1 mg/mL	BLOQ	3.7	9.7	BLOQ	9.4	2699.3	30.0	17.1	36.7	234.5
0.21 mg/mL	BLOQ	9.9	16.9	14.2	1.2	245.8	24.3	34.7	BLOQ	BLOQ
0.021 mg/mL	BLOQ	BLOQ	12.0	BLOQ	4.0	10.5	1.7	8.7	BLOQ	BLOQ
21 mg/mL + LPS	124.9	BLOQ	25.8	2.1	6.9	74.6	16.5	17.8	28.1	BLOQ
2.1 mg/mL + LPS	BLOQ	12.9	20.4	BLOQ	7.9	5382.2	42.5	6.0	120.8	916.6
0.21 mg/mL + LPS	73.2	633.9	26.1	6.3	3.1	3745.4	74.9	BLOQ	59.4	1161.0
0.021 mg/mL + LPS	324.4	1409.6	22.3	BLOQ	12.9	1628.7	29.4	9.6	20.7	1122.9

Analysis and Conclusions

NCL150-3 induced high levels of IL-8 in vitro, and triggered low levels of TNFα only when tested at 2.1 mg/mL. The combination NCL150-3 and lipopolysaccharide treatment resulted in marked suppression of LPS-induced pyrogenic cytokines (TNFα and IL-1β) and IFNγ, while it enhanced IL-8 production. This data suggest that NCL150-3 possess immunosuppressive properties, and is in agreement with other tests presented in this report and demonstrating an immunosuppressive potential of NCL150-3 (suppression of mitogen-induced T-cell proliferation (Figure IV-5), antigen-specific T-cell proliferation (Figure IV-6), and pyrogen-induced cytokine marker (Figure I-1)).

Induction of IL-8 and enhancement of inflammation-triggered IL-8 secretion observed in this study with NCL150-3 is not unique to this formulation and has been reported for a variety of immunosuppressive agents (e.g. cyclosporine A and tacrolimus) which function through inhibition of calcium- and calmodulin-dependent calcineurin activation, and the autophagy inhibitor rapamycin [10, 11]. Immunosuppressive agents acting through different mechanisms (e.g. dexamethasone) do not share this property [11].

Due to limited quantities, this study did not include NCL149-1, the void polymeric nanoformulation; therefore we cannot conclude which part of the formulation (curcumin or polymer) is responsible for the observed immunosuppression. Since curcumin loading is low and the polymer demonstrated strong immunosuppressive properties in other tests (Figure IV-6), it is likely that the polymeric part of the formulation is the main immunosuppressive component of NCL150-3. However, it is also possible that curcumin contributes to this; curcumin has been reported to enhance immunosuppressive properties of cyclosporine [12].

Effects on Cytotoxicity of NK cells (ITA-11)

Design and Methods

The objective of this experiment was to evaluate the nanoparticles' ability to inhibit cytotoxicity of natural killer (NK) cells *in vitro*. The experiment was conducted according to the NCL protocol ITA-11. NCL150-3 was tested at four concentrations: 0.021, 0.21, 2.1 and 21.0 mg/mL of nanocurcumin.

Results

NCL150-3 demonstrated inhibition of NK cytotoxicity at two tested concentrations (2.1 and 21 mg/mL) (Figure IV-9).

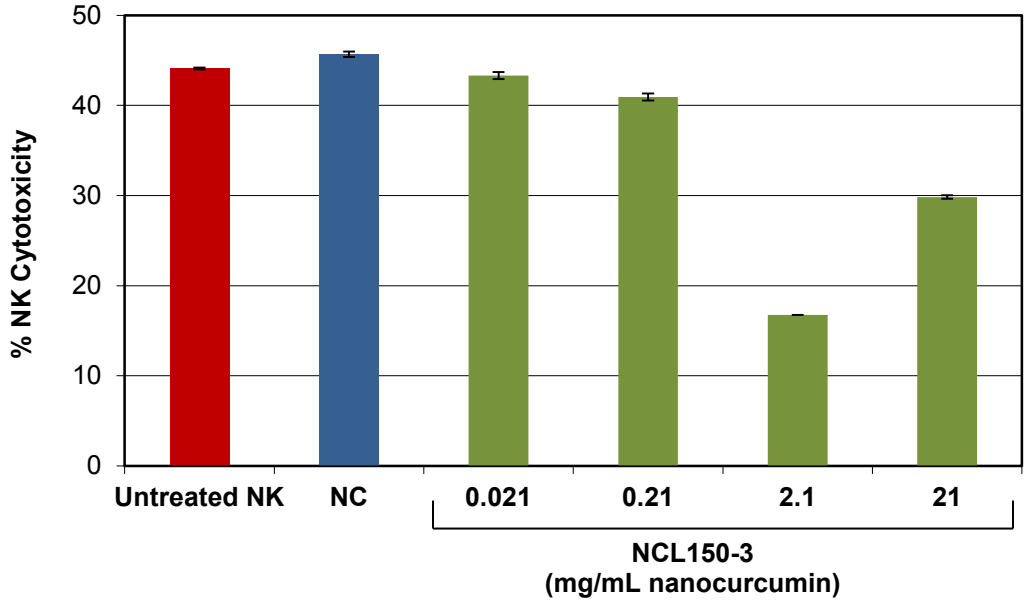

Figure IV-9. Cytotoxicity of NK cells (ITA-11). NK cells were either untreated, or treated with negative control (PBS) or NCL150-3 at four concentrations for 24 h. After several washes to remove excess particles or other treatments, NK cells were co-cultured for an additional 24 h with the cancer cell line HepG2. Viability of HepG2 cells was monitored in real-time using an RT-CES instrument. Areas under the curve were used to calculate percent cytotoxicity. Shown is the mean of duplicate measurements (CV<25%).

Analysis and Conclusions

NCL150-3 inhibited cytotoxicity of NK cells. This data suggests that NCL150-3 may have immunosuppressive properties, in agreement with other results presented in this report (Figures I-1, IV-5, IV-6 and Table IV-1).

V. Pharmacokinetics and Metabolism in Bile Duct Cannulated Rats

Section Summary

The objective of this study was to compare the pharmacokinetics and metabolism of polymeric nanoparticle encapsulated nanocurcumin (NCL150-3), and solvent solubilized curcumin formulations in Sprague Dawley (SD) rats. Nanocurcumin is currently under development for cancer therapy. The second objective of this study was to utilize the metabolic instability of curcumin to assess *in vivo* drug release from nanocurcumin. Since free, unencapsulated curcumin is rapidly metabolized and excreted in rats upon i.v. administration, only nanoparticle encapsulated curcumin can be detected in plasma samples. Measured curcumin concentrations were assumed part of the nanoformulation and were used to estimate the concentration of the nanocurcumin formulation. Measured metabolite concentrations were used to estimate the concentration of any unencapsulated curcumin.

Nanocurcumin and solvent solubilized curcumin were administered at 10 mg curcumin/kg by jugular vein to bile duct-cannulated male SD rats (n = 5). Nanocurcumin increased the plasma C_{max} of curcumin 1749-fold relative to the solvent solubilized curcumin. Nanocurcumin also increased the relative abundance of curcumin and glucuronides in bile, but did not dramatically alter urine and tissue metabolite profiles. The observed increase in biliary and urinary excretion of both curcumin and metabolites for the nanocurcumin formulation suggested rapid, “burst” release of curcumin. Although the burst release observed in this study is a limitation for *targeted* tumor delivery, nanocurcumin still exhibits major advantages over solvent solubilized curcumin; the nanoformulation does not result in the lung accumulation observed for the solvent solubilized curcumin and increases overall systemic curcumin exposure.

Design & Methods

Background and Study Objective

Curcumin is a natural diphenolic compound derived from turmeric (*Curcuma longa*), which is currently undergoing evaluation as a chemopreventive and anticancer agent [1]. Curcumin principally acts as a chemosensitizer, improving the combinatorial efficacy with conventional cytotoxic agents, like gemcitabine and doxorubicin [13, 14]. Curcumin's clinical application has thus far been limited by low solubility, low bioavailability, rapid metabolism, and degradation at physiological pH [15]. While curcumin is stable under acidic conditions, and plasma proteins can help to stabilize curcumin, it rapidly degrades to vanillin, ferulic acid, and vanillylidenacetone at pH ≥ 6.8 (Figure V-1A) [16]. In animal models, curcumin is rapidly metabolized into tetrahydrocurcumin (THC) and hexahydrocurcumin (HHC), and their sulfate and glucuronide conjugates (Figure V-1B), which are excreted into bile and urine [17, 18]. Numerous curcumin nanoformulations have been developed to increase oral absorption, systemic exposure (AUC, C_{max}) and mean residence time (MRT) of entrapped curcumin [15, 19-23]. However, it is still unknown if the nanoformulations alter the metabolite profile or excretion pathways of curcumin. Altered metabolism resulting from curcumin nanoformulation could be important. Some studies have suggested that certain metabolites, such as THC and phenolic glucuronides, are biologically active and may be responsible for at least some of the pharmacology attributed to curcumin [24, 25].

Drug release kinetics is one of the critical factors which determine ADME of nanoformulated drugs [26]. Targeted drug delivery systems require controlled and sustained release kinetics. The release kinetics of nanoformulated drugs are usually evaluated using in vitro release assays. However, traditional in vitro release assays have been demonstrated to be a poor predictor of in vivo release. For example, nanoformulated drugs exhibiting sustained in vitro release have been found to be rapidly released in vivo [27]. Furthermore, it is difficult to measure *in vivo* drug release kinetics since most current sample preparation methods (e.g., liquid-liquid extraction, solid phase extraction, and protein precipitation) cannot accurately distinguish encapsulated drug vs. free drug in blood and tissue matrices [28]. Due to metabolic instability, free, unencapsulated curcumin released from nanoformulations in vivo is rapidly metabolized and excreted, with encapsulated curcumin accounting for the majority of total curcumin measured in vivo. Curcumin and metabolites, therefore, can be used to estimate nanoparticle encapsulated and unencapsulated fractions, respectively, allowing assessment of *in vivo* drug release without requiring bioanalytical methods that distinguish encapsulated and unencapsulated drug.

The objectives of this study were to: (1) determine the effects of polymeric nanoparticle encapsulation (nanocurcumin) on the metabolite profile, excretion, and tissue distribution of curcumin; (2) assess the in vivo release of curcumin from nanocurcumin. The pharmacokinetic and metabolic profiles, biliary and urinary excretion, and tissue distribution of nanocurcumin and solvent solubilized curcumin were evaluated in bile duct-cannulated rats. Additionally, *in vivo* release of curcumin from nanocurcumin was assessed by quantifying both curcumin and its metabolites in plasma, tissues, bile, urine, and feces.

A.

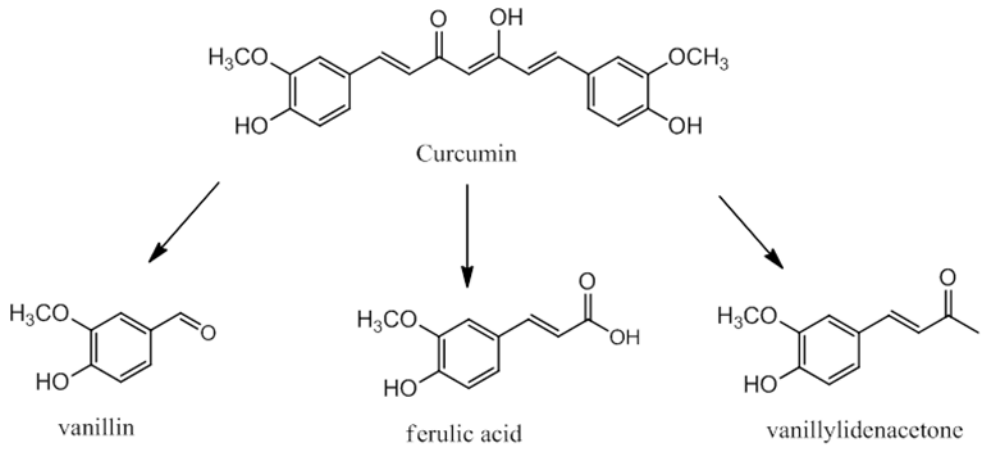

B.

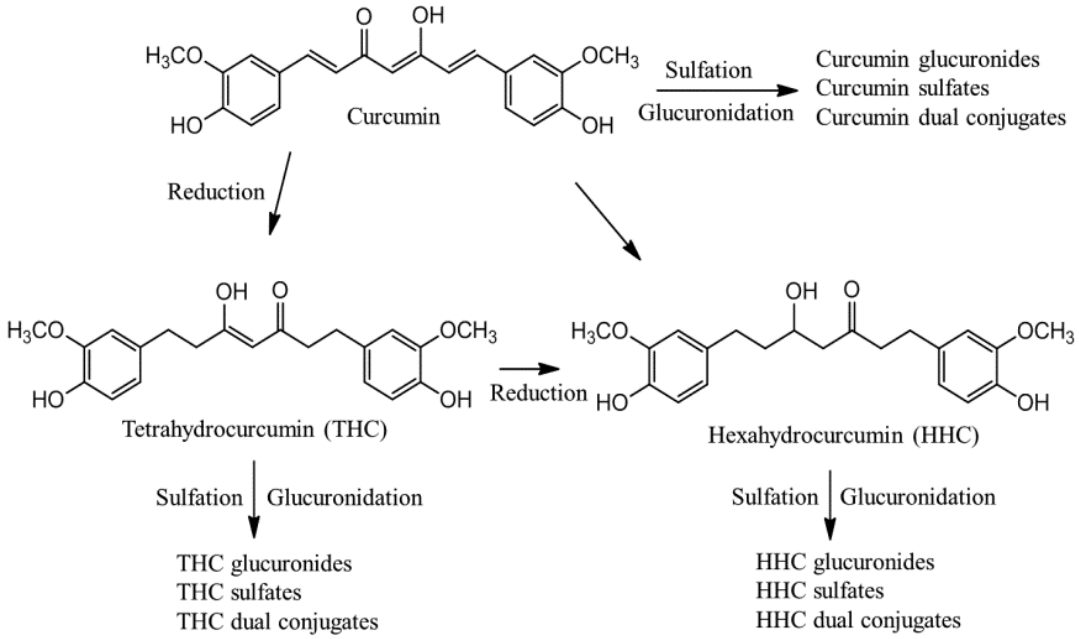

Figure V-1. Curcumin metabolite structures. (A) Degradation pathways of curcumin in PBS [16]. **(B)** Metabolic pathways of curcumin in rats [29, 30].

Experimental Methods

Materials

High purity synthetic curcumin (>99%) was purchased from Axxora (Farmingdale, NY). Curcumin-glucuronide was purchased TLC PharmaChem (Vaughan, Canada). Tetrahydrocurcumin (THC), hexahydrocurcumin (HHC), bisdemethoxycurcumin, vanillylidenacetone, β-glucuronidase from *Escherichia coli* (5 million units/g protein), sulfatase from *Helix pomatia* (sulfatase > 10,000 units/g protein, β-glucuronidase > 300,000 units/g protein), monomers and reagents for polymer nanoparticle synthesis, specifically N-isopropylacrylamide (NIPAAM), vinylpyrrolidone (VP), acrylic acid (AA), N, N′-methylenebis-acrylamide, ammonium persulfate, and ferrous sulfate were obtained from Sigma (St. Louis, MO). MI-129 was a gift from Dr. Shaomeng Wang, University of Michigan. BD Vacutainer, PTS gel lithium heparin plus blood collection tubes were purchased from Moore Medical (New Britain, CT). Formic acid (LC-MS grade), acetonitrile (LC-MS grade), and ammonium acetate were purchased from Fisher Scientific (Pittsburgh, PA). Filter units (0.2 µm pore size) were obtained from Millipore (Billerica, MA).

Stability Assay

Nanocurcumin and curcumin stock solutions were diluted in PBS, citric acid-adjusted PBS buffer (PBS pH was adjusted to 5.7 using citric acid), and rat plasma in triplicate to give a final curcumin concentration of 2 µg/mL. The solutions (1 mL) were incubated at 37°C for 1 h and an aliquot of 50 µL of solution was collected at 0, 5, 10, 15, 30, 45, and 60 min. Protein was precipitated with 150 µL of ice-cold acetonitrile containing internal standards, bisdemethoxycurcumin (500 ng/mL) and MI-129 (500 ng/mL). The samples were centrifuged at 14,000 rpm for 10 min and 10 µL of supernatant was analyzed by the LC-vis-MS method described later in this section.

To assess the stability of curcumin in dosing solutions of nanocurcumin (equivalent to 2.5 mg curcumin /mL in PBS) and solvent solubilized curcumin (5 mg/mL in DMSO/PBS 1:1 (v/v)), an aliquot of both dosing solutions was kept at room temperature for 48 h. The degradation of curcumin was monitored by the LC-Vis-MS method below. To ensure DMSO/PBS curcumin did not aggregate in plasma, curcumin dosing solution (5 mg/mL) was diluted 10, 20, and 50-fold with rat plasma. The particle size of possible aggregates was measured in triplicate by the Zetasizer Nano ZS.

Husbandry

NCI-Frederick is accredited by AAALAC International and follows the Public Health Service *Policy for the Care and Use of Laboratory Animals* (Health Research Extension Act of 1985, Public Law 99-158, 1986). Animal care was provided in accordance with the procedures outlined in the *Guide for Care and Use of Laboratory Animals* (National Research Council, 1996; National Academy Press, Washington, D.C.). All animal protocols were approved by the NCI-Fredrick institutional Animal Care and Use Committee. The experiments outlined herein are scientifically justified and do not represent an unnecessary duplication of previous work by the sponsor.

Pharmacokinetic Studies

Twelve double jugular catheterized and bile duct cannulated male Sprague-Dawley (SD) rats (65 days old, approximate weight of 300 g) were purchased from Charles River Laboratories, Inc. (Raleigh, NC). The animals were placed in metabolic cages, fed standard rat food (Purina) and chlorinated tap water *ad libitum*. The animal rooms were maintained on a 12-h light/dark cycle, with a temperature range between 20° and 22°C, and 50% relative humidity.

Dosing solutions of nanocurcumin and solvent solubilized curcumin were freshly prepared and 10 mg curcumin /kg was administered via the left jugular vein catheter (n = 5) (Table V-1). A blank control group (n = 2) was treated with PBS (4 mL/kg). Blood samples (300 µL) were collected via the right jugular catheters at each time point (15 min, and 1, 2, 4, 8, 24, and 30 h postdose) and placed in lithium heparinized tubes. The blood was centrifuged (2000 g for 10 min) immediately to collect plasma. Bile samples were collected at 1 h increments for the first 8 h. Urine and feces were collected at 8 and 24 h intervals. Replacement saline was given subcutaneously (s.c.) for bile removed. All samples were weighed, frozen at -80°C, and protected from light.

Table V-1. Dosing Groups for Pharmacokinetic Study

Test Group	Rat #	Dose (mg DTX/kg)	Volume (mL/kg)	# of rats
NCL150-3	#1-5	10 mg	4	5
DMSO Curcumin	#6-10	10 mg	2	5
PBS control	#11-12	-	4	2

Tissue Distribution Studies

Thirteen single jugular catheterized male Sprague-Dawley (SD) rats (65 days old) were randomly divided into 5 groups. Group 1 (n = 3) and group 2 (n = 3) were administered nanocurcumin (equivalent to 10 mg curcumin/kg), while group 3 (n = 3) and group 4 (n = 3) were administered solvent solubilized curcumin (10 mg/kg) via the jugular vein catheter (Table V-2). Group 5 (n = 1) received PBS i.v. (4 mL/kg). The blood and tissue collection time point for groups 1, 3 and 5 was at 15 min and for groups 2 and 4 was 60 min. At each collection time point, rats were euthanized by CO_2 asphyxiation. Blood (1 mL) was collected in Li-heparinized tubes from cardiac puncture and spun (2000x*g* for 10 min) to collect plasma. Liver, lungs, kidneys, heart and spleen were collected, washed in ice cold pH 5.7 citric acid-PBS buffer, blotted dry, weighed, and frozen at -80°C.

Table V-2. Dosing Groups for Tissue Distribution Study

Test Group	Rat #	Dose (mg DTX/kg)	Volume (mL/kg)	Time (min)	# of rats
NCL150-3	#1-3	10 mg	4	15	3
NCL150-3	#4-6	10 mg	4	60	3
DMSO Curcumin	#7-9	10 mg	2	15	3
DMSO Curcumin	#9-12	10 mg	2	60	3
PBS control	#13	-	4	15	1

Analytical Sample Preparation

Plasma: β-glucuronidase and sulfatase stock solutions were prepared in pH 5.7 citric acid-PBS buffer at concentrations of 50,000 units/mL and 1000 units/mL, respectively. Rat plasma sample (40 µL aliquots) and 3 µL of 0.25 M citric acid were added to each microcentrifuge tube in triplicate. An aliquot (7 µL) of β-glucuronidase solution or sulfatase solution was added to the three tubes. After incubation at 37°C for 1 h, the samples were mixed with 150 µL of ice-cold acetonitrile containing 0.1% formic acid and two internal standards, bisdemethoxycurcumin (500 ng/mL) and MI-129 (500 ng/mL). The samples were placed in a freezer (-20°C) for 10 min and then centrifuged at 14,000 rpm for 10 min at 4°C. The supernatants were analyzed by the LC-Vis-MS method below.

Urine: Rat urine sample (50 µL aliquots) and 3 µL of 0.5 M citric acid were added to each microcentrifuge tube in triplicate. An aliquot (7 µL) of β-glucuronidase solution or sulfatase solution was added to the three tubes. After incubation at 37°C for 1 h, the samples were mixed with 180 µL of ice-cold acetonitrile containing 0.1% formic acid and the above mentioned internal standards. Similar procedures described above for plasma samples were applied to urine samples.

Bile: Rat bile sample (60 µL aliquots) and 10 µL of 0.1 M citric acid were added to each microcentrifuge tube in triplicate. An aliquot (10 µL) of β-glucuronidase solution or sulfatase solution was added to the three tubes. After incubation at 37°C for 1 h, the samples were mixed with 240 µL of ice-cold acetonitrile containing 0.1% formic acid and internal standards. Similar procedures described above for plasma samples were applied to bile samples.

Feces: Feces were mixed with acetonitrile containing 0.1% formic acid and internal standards to a concentration of 0.1 g/mL. The mixture was vortexed until the feces were homogenized, sonicated for 5 min, then centrifuged 4000 rpm for 10 min. Supernatant (0.5 mL) was evaporated in a microcentrifuge tube to dryness under nitrogen in triplicate, and the residue was dissolved in pH 5.7 citric acid-PBS buffer (50 µL). An aliquot (10 µL) of β-glucuronidase solution or sulfatase solution was added to the three tubes. After incubation at 37°C for 1 h, the samples were mixed with 180 µL of ice-cold acetonitrile containing 0.1% formic acid. Similar procedures described above for plasma samples were applied to feces samples.

Tissues: Tissue samples were accurately weighed and homogenized in four volumes (w/v) of pH 5.7 citric acid-PBS buffer using a Polytron PT1300D homogenizer (Kinematica,Inc., Bohemia, NY). Tissue homogenate (50 µL) and 3 µL of 0.25 M citric acid were added to each microcentrifuge tube in triplicate. An aliquot (7 µL) of β-glucuronidase solution or sulfatase solution was added to the three tubes. After incubation at 37°C for 1 h, the samples were mixed with 180 µL of ice-cold acetonitrile containing 0.1% formic acid and two internal standards.

Validation of enzymatic hydrolysis: To ensure efficient and complete hydrolysis of conjugates, curcumin-glucuronide standard was spiked into blank plasma, urine, bile, feces and tissue homogenates at 40 µg/mL and 100 µg/mL and incubated with β-glucuronidase or sulfatase (containing β-glucuronidase > 300,000 units/g) as described above. After incubation, the remaining curcumin-glucuronide and formed curcumin were quantified. Since curcumin-sulfate standard is not commercially available, the validation of sulfate hydrolysis was not conducted. The complete hydrolysis of sulfates was confirmed by the disappearance of the chromatographic peaks identified as sulfates in unknown samples.

LC-Vis-MS Analysis

LC-Vis-MS analysis of curcumin metabolites (Figure V-2) was performed using an LC-MS 2020 system equipped with a UV/Vis detector (Shimadzu, Columbia, MD). Separation was performed on a Zorbax SB-C18 column of the dimensions 4.6 × 150 mm and a particle size of 5 µm (Agilent) coupled with a guard column (4.6 × 12.5 mm). The analytes (injection volume 10 µL) were separated by a binary gradient at a flow rate of 1 mL/min of 10 mM ammonium acetate containing 0.1% formic acid as solvent A and acetonitrile containing 0.1% formic acid as solvent B. For plasma, urine and tissue sample analysis, the following linear gradients were used: 0 min, 30% B; 3 min, 30% B; 11 min, 60% B; 13 min, 60% B; 13.5 min, 90% B; 15 min, 90% B; 15.01 min, 30% B; and 19 min, 30% B. For bile sample analysis, the following gradient was used: 0 min, 30% B; 3 min, 30% B; 18 min, 55% B; 20 min, 90% B; 20.01 min, 30% B; and 24 min, 30% B. Column temperature and sample temperature were maintained at 30° and 4°C, respectively. Curcumin and curcumin glucuronide were detected using a UV/Vis detector operating at 425 nm, and bisdemethoxycurcumin served as an internal standard (IS) for LC-UV/Vis analysis. THC, HHC and vanillylidenacetone were detected using positive ESI MS in selected ion monitoring mode and MI-129 was used as an IS for LC-MS analysis. MS parameters for THC, HHC, and vanillylidenacetone were optimized by injecting 10 µg/mL of analyte solutions and are shown in Table V- 3.

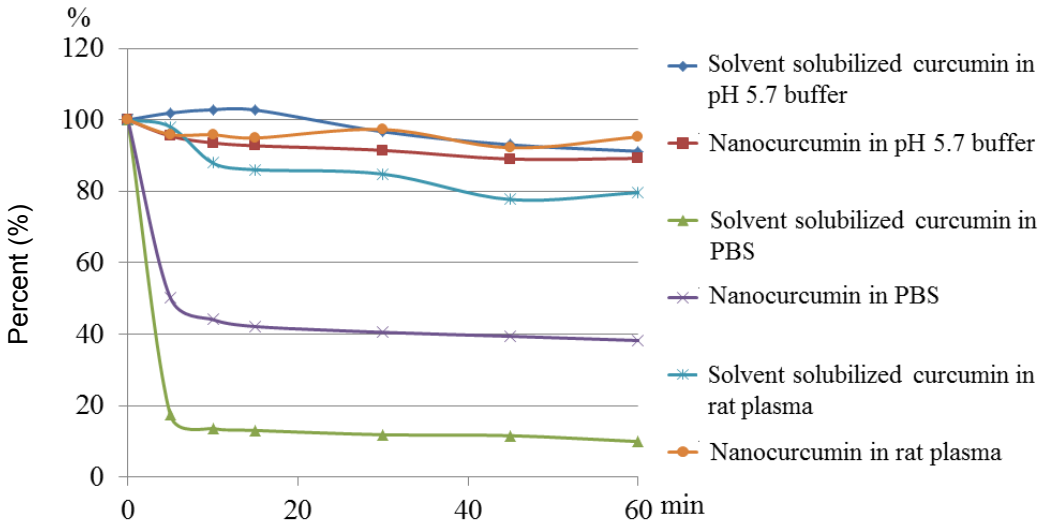

Figure V-2. Stability of solvent solubilized curcumin and nanocurcumin. Stability of solvent solubilized curcumin and nanocurcumin (2 µg/mL curcumin) in pH 5.7 buffer, pH 7.3 PBS buffer and rat plasma.

Table V-3. Mass spectrometer parameters.

Parameters	Tetrahydrocurcumin	Hexahydrocurcumin	Vanillylidenacetone
Interface Temperature (°C)	350	350	350
DL Temperature (°C)	300	300	300
Heat Block (°C)	400	400	400
Nebulizing Gas Flow (L/min)	1.5	1.5	1.5
Dry Gas Flow (L/min)	15	15	15
m/z	373.4	375.4	193.2
Interface Voltage (kV)	4.5	4.5	4.5
DL Voltage (V)	0	0	0
Qarray DC (V)	0	0	0

Calibration and Method Validation.
Calibration standards for each analyte were prepared in tissue, plasma, bile, urine, and feces matrices from naïve untreated rats. The calibration standards in each matrix were worked up for LC-Vis-MS analysis in the exact procedures as described for the unknown samples. An equivalent amount of IS was added to both unknown samples and calibration standards before LC-Vis-MS analysis. Blank samples were interspersed in the sequence to ensure no inter-sample carryover was occurring. LC-UV/Vis and LC-MS methods were validated for LOQs, linearity of calibration curves, specificity, precision, accuracy, and recovery in various matrices. For each analyte, the LOQ values were determined using signal-to-noise (S/N) = 10. See Table V-4 for the LOQ values of curcumin, THC, HHC, and vanillylidenacetone in various matrices. The linearity ranges of calibrations curves are shown in Table V-5. The precision and accuracy of the methods were determined by repeated analysis of the quality control samples (QCs) prepared from a separate stock solution at low, medium and high concentrations. The precision of the methods was evaluated by the relative standard deviations (RSD) with replicate assays (n = 5), and the accuracy of the methods was evaluated based on the error of the assayed QCs (n = 3) relative to their spiked concentrations (RE).To determine extraction recovery, blank sample and post-extracted blank sample were spiked with analytes at three concentrations (n = 3). The results of precision, accuracy, and extraction recovery in various matrices are shown in Table V-6 and Table V-7.

Table V-4. LOQs of curcumin, tetrahydrocurcumin, hexahydrocurcumin and vanillylidenacetone in biofluids and tissue homogenates (µg/mL).

Matrix	Curcumin	Tetrahydrocurcumin	Hexahydrocurcumin	Vanillylidenacetone
Plasma	0.01	0.5	0.25	0.2
Bile	0.02	2	0.5	1
Urine	0.02	2.5	1	1
Feces	0.02	2	1	0.5
Lung	0.02	2	0.4	0.4
Liver	0.02	2	0.4	0.4
Spleen	0.02	1	0.4	0.2
Heart	0.01	1	0.2	0.2
Kidneys	0.02	1	0.2	0.2

Table V-5. Calibration curves of curcumin, tetrahydrocurcumin, hexahydrocurcumin and vanillylidenacetone in biofluids and tissue homogenates (µg/mL).

Matrix	Linearity range (R^2 >0.99 for all samples)			
	Curcumin	Tetrahydrocurcumin	Hexahydrocurcumin	Vanillylidenacetone
Plasma	0.01-10	1-200	0.5-200	0.2-200
Bile	0.02-50	2-200	1-200	1-200
Urine	0.02-10	2.5-50	1-50	1-50
Feces	0.02-10	2-50	1-50	0.5-50
Lung	0.1-100	2-200	1-200	0.5-100
Liver	0.05-5	2-50	0.5-50	0.5-50
Spleen	0.05-10	1-50	0.5-50	0.5-50
Heart	0.01-5	1-50	0.5-50	0.5-50
Kidneys	0.02-5	1-50	0.5-50	0.5-50

Table V-6. Precision, accuracy and recovery of curcumin in biofluids and tissue homogenates.

Matrix	Spiked concentration (μg/mL)	Precision (RSD%) (n = 5)	Accuracy (RE%) (n = 3)	Recovery (%) (n = 3)
Plasma	0.02 0.5 10	8.7 4.6 6.9	5.2 -2.1 3.0	89.3±10.1 91.9±5.3 93.1±6.4
Bile	0.05 1 50	8.6 6.9 5.3	-6.5 0.9 -4.2	92.3±7.5 102.4±6.1 95.8±4.2
Urine	0.05 0.5 10	10.5 4.3 5.9	7.4 5.1 3.9	85.2±9.4 91.8±7.3 92.5±5.2
Feces	0.05 0.5 10	8.5 6.8 9.0	-5.7 6.1 -4.9	87.1±9.9 93.5±5.4 90.1±6.2
Lung	0.1 2 100	5.1 2.4 3.6	5.5 7.8 2.1	93.0±4.7 89.0±7.9 95.2±6.8
Liver	0.05 0.5 5	6.2 3.3 4.9	7.4 -6.9 -3.7	107.1±8.5 98.2±7.6 96.9±7.9
Spleen	0.05 0.5 10	8.9 3.6 5.8	-6.0 -4.9 5.6	88.5±7.4 93.9±4.6 99.1±6.3
Heart	0.02 0.5 5	11.2 6.7 4.1	7.9 7.4 -3.6	107.4±8.8 104.1±6.9 94.8±7.3
Kidneys	0.05 0.5 5	9.9 4.8 7.1	-7.7 6.2 3.5	90.3±12.5 89.5±6.4 94.2±6.0

Table V-7. Precision, accuracy and recovery of tetrahydrocurcumin, hexahydrocurcumin and vanillylidenacetone in biofluids and tissue homogenates.

Compounds	Matrix	Spiked concentration (µg/mL)	Precision (RSD%) (n = 5)	Accuracy (RE%) (n = 3)	Recovery (%) (n = 3)
Tetrahydrocurcumin	Plasma	1	11.6	-7.5	82.1±8.6
		20	7.2	-3.9	84.2±7.1
		200	5.9	7.2	85.8±8.4
	Bile	2	11.4	10.9	80.4±9.3
		20	6.3	-5.8	86.7±7.9
		200	7.9	6.1	84.5±6.8
	Urine	2.5	9.3	-9.7	86.7±9.2
		10	8.1	7.1	89.6±10.4
		50	5.2	7.8	86.0±5.8
Hexahydrocurcumin	Plasma	1	10.3	-8.9	84.8±9.9
		20	7.8	6.8	80.4±7.3
		200	8.2	-5.5	86.6±4.9
	Bile	2	11.2	9.2	81.2±7.6
		20	7.9	-6.4	83.7±5.5
		200	6.1	-7.3	82.3±8.1
	Urine	2	9.5	-8.5	88.1±9.0
		10	8.9	7.4	84.5±7.2
		50	8.4	8.2	85.9±6.4
	Liver	1	9.3	-6.5	80.6±8.5
		10	9.7	7.9	83.6±8.9
		50	7.6	-5.7	82.5±7.1
Vanillylidenacetone	Plasma	0.5	11.4	8.4	85.1±9.2
		20	7.3	-6.7	82.6±7.9
		200	8.6	-7.2	87.2±6.8

Data Analysis

For each analyte, three concentrations were determined: the concentration without sample hydrolysis (C1), the concentration after hydrolysis of glucuronides (C2), and the concentration after hydrolysis of both sulfates and glucuronides (C3). The total concentration of curcumin glucuronides was calculated as C2 - C1, while the total concentration of sulfates and sulfate/glucuronide dual conjugates was calculated as C3 – C2. The concentrations of THC and HHC conjugates were calculated following the same procedures. The concentrations of curcumin and its metabolites were presented as ng/mL or percentage of injected dose (%ID). The %ID of curcumin in plasma, bile and urine was calculated as:

$$\frac{(\text{curcumin concentration} \times \text{volume of plasma, bile or urine}}{\text{Total dose}} \times 100\%$$

The %ID of curcumin in tissues was calculated as:

$$\frac{(\text{tissue curcumin concentration} \times \text{tissue mass})}{\text{Total dose}} \times 100\%.$$

The volumes of bile and urine at each time point were experimentally measured. The total plasma volume and tissue masses were calculated using rat body weight and previously reported rat physiological parameters [31]. The %ID of each metabolite was calculated using molar concentration. The relative abundance of each metabolite in bile and urine was calculated as:

$$\frac{\text{the molar amount of individual metabolite}}{\text{the sum of molar amount of curcumin and metabolites}} \times 100\%.$$

WinNonlin Version 4.1 (Pharsight, Mountain View, CA) was used to calculate pharmacokinetic parameters by noncompartmental analysis.

Results

Stability in Buffers, Rat Plasma and Dosing Solutions

In pH 5.7 buffer, both solvent solubilized curcumin (2 µg/mL) and nanocurcumin (equivalent to 2 µg/mL curcumin) were stable (Figure V-2). In contrast, approximately 60% of nanocurcumin and 90% of solvent solubilized curcumin decomposed after 1 h incubation in PBS (pH 7.4). Rat plasma proteins stabilized both nanocurcumin and solvent solubilized curcumin. Nanocurcumin exhibited high stability in the dosing solution (269 mg polymer/mL, equivalent to 2.5 mg curcumin /mL, in pH 7.4 PBS), with 98.2 ± 8.8% curcumin remaining after storage at room temperature for 48 h, suggesting that the degradation rate of nanoformulated curcumin in PBS is concentration-dependent. Similarly, solvent solubilized curcumin (5 mg/mL) showed improved stability in mixed DMSO/PBS (1:1, v/v) dosing solution, with 84.2 ± 10.2% curcumin detected after 48 h storage at room temperature. To ensure there was no curcumin aggregation in the blood stream upon i.v. administration of the solvent solubilized curcumin dosing solution, the dosing solution was diluted 10, 20, and 50-fold with rat plasma. The average hydrodynamic sizes of blank rat plasma and the three diluted solutions are shown in Figure V-3. The peaks at 300 nm were likely due to the platelet-derived microparticles in rat plasma [32]. No curcumin aggregation (peaks > 1000 nm) was observed by dynamic light scattering (DLS) after 10, 20, and 50-fold dilution with rat plasma.

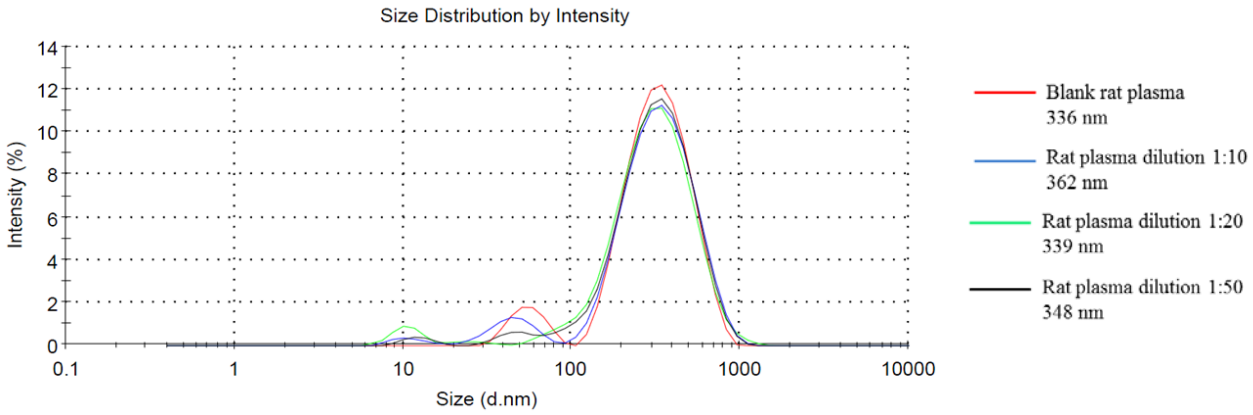

Figure V-3. Effect of rat plasma dilution on the aggregation of solvent solubilized curcumin. Solvent solubilized curcumin (5 mg/mL in DMSO/PBS, 1:1, v/v) was diluted 10, 20, and 50-fold with rat plasma. The figure shows the average curve from three measurements. No aggregation of curcumin was observed. The peaks at 300-400 nm were likely due to the platelet-derived microparticles in rat plasma.

Plasma Concentration Profiles

Under the optimized hydrolysis assays, both glucuronides and sulfates in various matrices were completely hydrolyzed by their corresponding enzymes. The hydrolysis yields were between 80-100%. Figure V-4, for example, shows complete hydrolysis of curcumin glucuronide in bile with an average hydrolysis yield (n = 3) of 87.4 ± 5.0%.

As shown in the plasma concentration profiles, curcumin was dominant in the plasma of the nanocurcumin group (Figure V-5A) while phase II conjugates were dominant in the plasma of solvent solubilized curcumin group (Figure V-5B). The C_{max} of curcumin for the nanocurcumin group was 25.50 ± 5.94 µg/mL (n = 5), while curcumin was only detectable at 15 min for the solvent solubilized curcumin group (14.6 ± 4.2 ng/mL, n = 5). The nanoformulation increased the plasma C_{max} of curcumin by 1749-fold. The nanoformulation also increased the plasma C_{max} of HHC conjugates and curcumin conjugates by 4.0 and 9.9-fold, respectively. THC conjugates, while present in the plasma of nanocurcumin treated animals, were not detectable for the solvent solubilized curcumin group (LOQ = 0.5 µg/mL). The curcumin Vd_{ss} for the nanocurcumin group was 320 ± 39 mL/kg (Table V-8), which is much larger than the rat plasma volume of 31.2 mL/kg [31], suggesting tissue distribution or metabolism of the nanoformulated curcumin. To better understand the distribution of the nanoformulated curcumin, the plasma concentration profiles are presented as the percentage of injected dose (%ID) for each treatment group (Figure V-6). For the nanocurcumin group and solvent solubilized curcumin group, 8.0 ± 1.8% and 0.01 ± 0.01% of injected dose were detected, respectively, as curcumin in the plasma at 15 min.

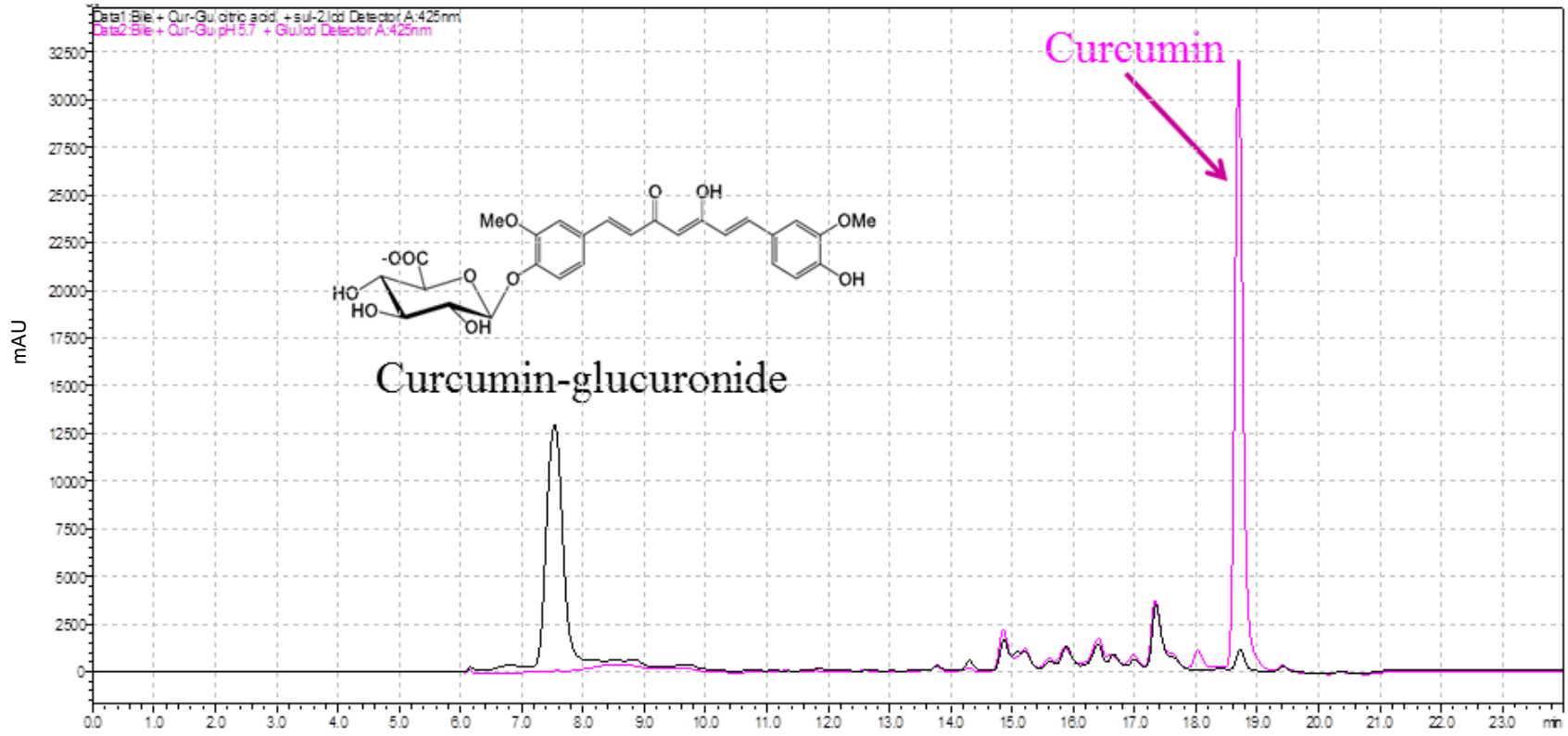

Cur-Glu: 40 µg/mL (73.5 µM)
Curcumin: 1). 25.2 µg/mL (68.4 µM); 2). 22.7 µg/mL (61.6 µM); 3). 23.1 µg/mL (62.7 µM)
Hydrolysis yield = 87.4 ± 5.0%

Figure V-4. Complete hydrolysis of curcumin-glucuronide by β-glucuronidase. Curcumin-glucuronide (40 µg/mL) was incubated with 100 units of β-glucuronidase at 37°C for 1 h in triplicate. The average hydrolysis yield was 87.4%. The black line shows the peak of curcumin-glucuronide and the pink line shows the peak of curcumin, for a representative incubation.

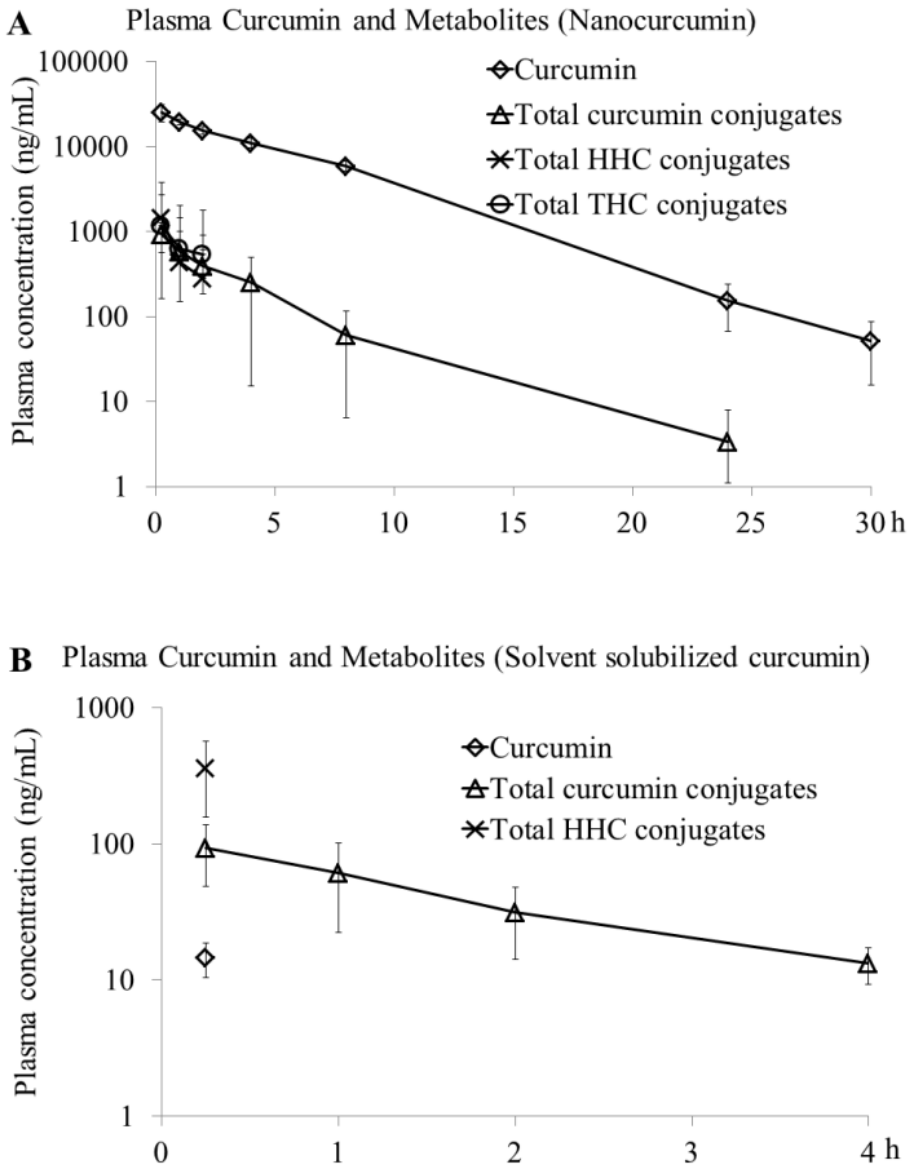

Figure V-5. Plasma concentration-time profiles of curcumin and its metabolites after i.v. administration of (A) nanocurcumin (equivalent to 10 mg/kg curcumin) and (B) solvent solubilized curcumin (10 mg/kg) to S-D rats. Each point represents the mean ± SD from n = 5 rats. For the nanocurcumin group, the plasma concentrations of THC conjugates and HHC conjugates were lower than the LOQs 4 h post dose. For the solvent solubilized curcumin group, the plasma concentrations of HHC conjugates and curcumin were lower than the LOQs 1 h postdose, and the plasma concentrations of curcumin conjugates were lower than the LOQ 8 h postdose. THC conjugates were not detectable in the plasma samples of the solvent solubilized curcumin group.

Table V-8. Pharmacokinetic parameters of nanoformulated curcumin in S-D rats (n = 5) derived by noncompartmental analysis.

PK parameters	Nanocurcumin Group
CL (mL/h/kg)	66 ± 7
AUC (h*ng/mL)	151135 ± 14106
MRT (h)	4.82 ± 0.35
$T_{1/2}$ (h)	3.19 ± 0.46
Vd_{ss} (mL/kg)	320 ± 39
C_{max} (ng/mL)	25499 ± 5937

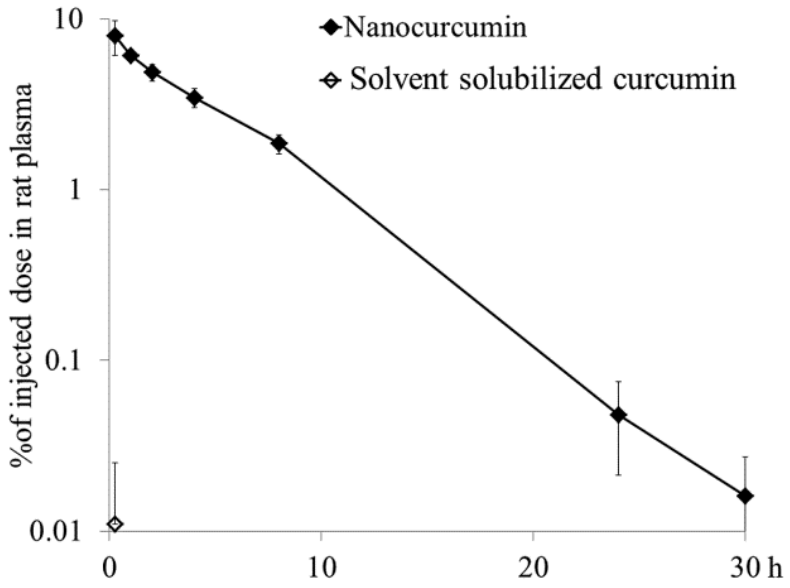

Figure V-6. **Plasma concentration-time profiles of curcumin presented as the percentage of injected dose (%ID) after i.v. administration of nanocurcumin (equivalent to 10 mg/kg curcumin) and solvent solubilized curcumin (10 mg/kg) to S-D rats.** Each point represents the mean ± SD from n = 5 rats. The %ID of curcumin in plasma was calculated as:

$$\frac{(\text{curcumin concentration} \times \text{total plasma volume})}{\text{Total dose}} \times 100\%$$

Biliary Excretion

The cumulative biliary excretion of curcumin and metabolites is presented as %ID. By 1 h postdose, 17.8 ± 3.9% (Figure V-7A) and 1.6 ± 1.1% (Figure V-7B) of the injected dose was excreted into bile for nanocurcumin and solvent solubilized curcumin groups, respectively. The rapid biliary excretion of curcumin metabolites for the nanocurcumin group implied burst release of curcumin. By 8 h postdose, 25.4 ± 1.7% and 4.4 ± 1.5% of the injected dose was excreted into the bile for the nanocurcumin and solvent solubilized curcumin groups, respectively. Nanoformulation increased the total biliary excretion of curcumin and metabolites by 5.7-fold. To demonstrate the effects of nanoformulation on the metabolite profile, the relative abundance of curcumin and metabolites excreted into bile during 0-8 h postdose are presented in Figure V-8. Rats 1-5 were treated with nanocurcumin and rats 6-10 were treated with solvent solubilized curcumin. For both groups, the major metabolites in bile were THC and HHC conjugates (totally > 80%). Free THC and HHC were not detectable. For the solvent solubilized curcumin group, concentrations of THC glucuronides were lower than the LOQ (2 µg/mL). Nanoformulation did not change the relative abundance of sulfates or dual conjugates of curcumin, THC and HHC in bile. However, the nanoformulation increased the relative abundance of curcumin and curcumin glucuronides by 2.9 and 7.9-fold, respectively. Due to bile duct cannulation, less than 0.01% of the injected dose was detected in feces over 24 h for both groups, which might have resulted from urine contamination.

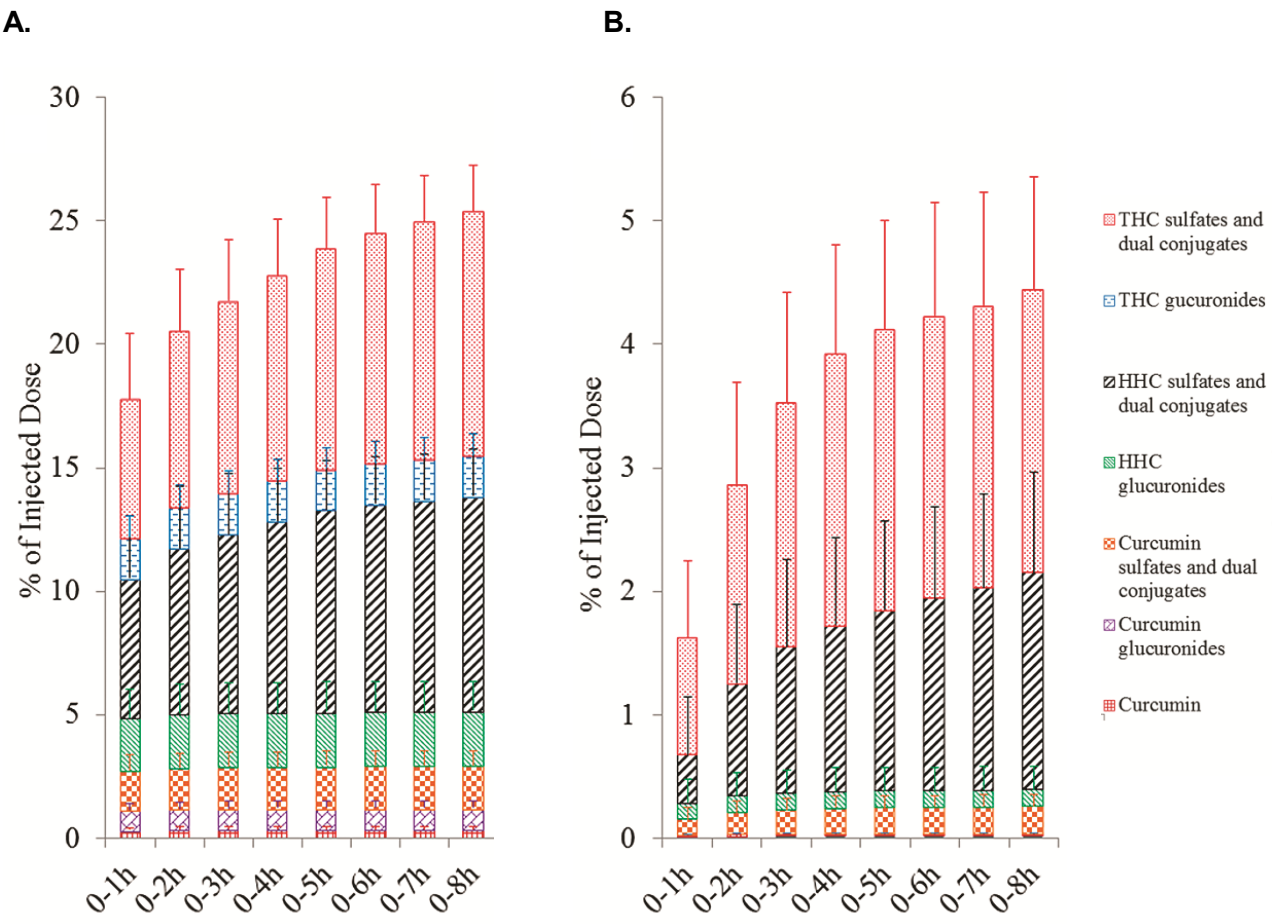

Figure V-7. Cumulative biliary excretion of curcumin and its metabolites after i.v. administration of (A) nanocurcumin (equivalent to 10 mg/kg curcumin) and (B) solvent solubilized curcumin (10 mg/kg) to S-D rats. Data are mean ± S.D., n = 5 rats. Bile samples were collected at 1 h intervals for the first 8 h. The %ID of curcumin and metabolites in bile was calculated as:

$$\frac{(\text{curcumin or metabolite concentration} \times \text{volume of collected bile})}{\text{Total molar dose}} \times 100\%$$

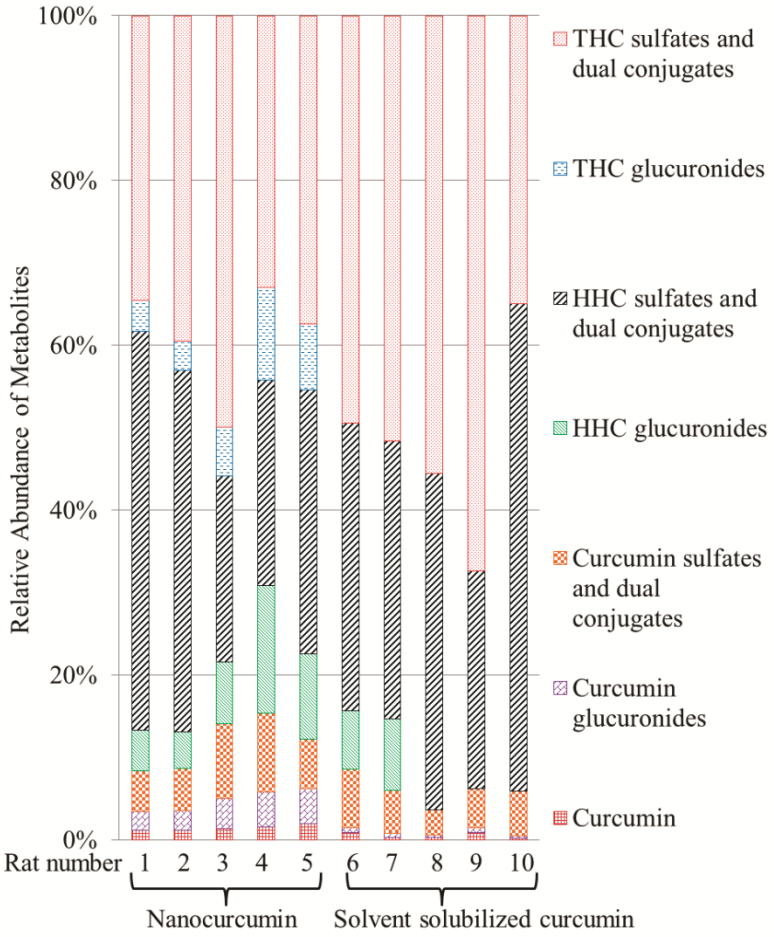

Figure V-8. Relative abundance of curcumin and its metabolites excreted into bile 0-8 h post i.v. administration of nanocurcumin (equivalent to 10 mg/kg curcumin) to rat 1-5 and solvent solubilized curcumin (10 mg/kg) to rat 6-10. The relative abundance of curcumin or metabolites in bile was calculated as:

$$\frac{\text{The molar amount of curcumin or individual metabolite in bile}}{\text{The sum of molar amount of curcumin and metabolites in bile}} \times 100\%$$

Urinary Excretion

The cumulative urinary excretion of curcumin and metabolites is presented as %ID. By 8 h postdose, 2.8 ± 3.0% (Figure V-9A) and 0.2 ± 0.2% (Figure V-9B) of the injected dose was excreted into the urine for the nanocurcumin and solvent solubilized curcumin groups, respectively. In total, 28.2% and 4.7% of injected dose was excreted into bile and urine during 0-8 h postdose for the nanocurcumin and solvent solubilized curcumin groups, respectively. By 24 h postdose, 3.0 ± 3.0% and 0.4 ± 0.1% of the injected dose accumulated in urine for the nanocurcumin group and solvent solubilized curcumin group, respectively. Nanoformulation increased total urinary excretion of curcumin and metabolites by 7.1-fold. Figure V-10 shows the relative abundance of curcumin and each metabolite excreted into urine during 0-24 h postdose. For both the nanocurcumin group (Rats 1-5) and the solvent solubilized curcumin group (Rats 6-10), the major metabolites in urine were HHC sulfates and dual conjugates (totally > 60%). HHC glucuronides (LOQ = 1 µg/mL) and THC conjugates (LOQ = 2.5 µg/mL) were not detected in urine for the solvent solubilized curcumin group. In contrast, HHC glucuronides were detected in urine for the nanocurcumin group (1.0 ± 1.3% of total amount of curcumin and metabolites in urine). The nanoformulation decreased the relative abundance of curcumin, curcumin glucuronides, and curcumin sulfates and dual conjugates in urine by 75.9%, 81.6% and 78.1%, respectively.

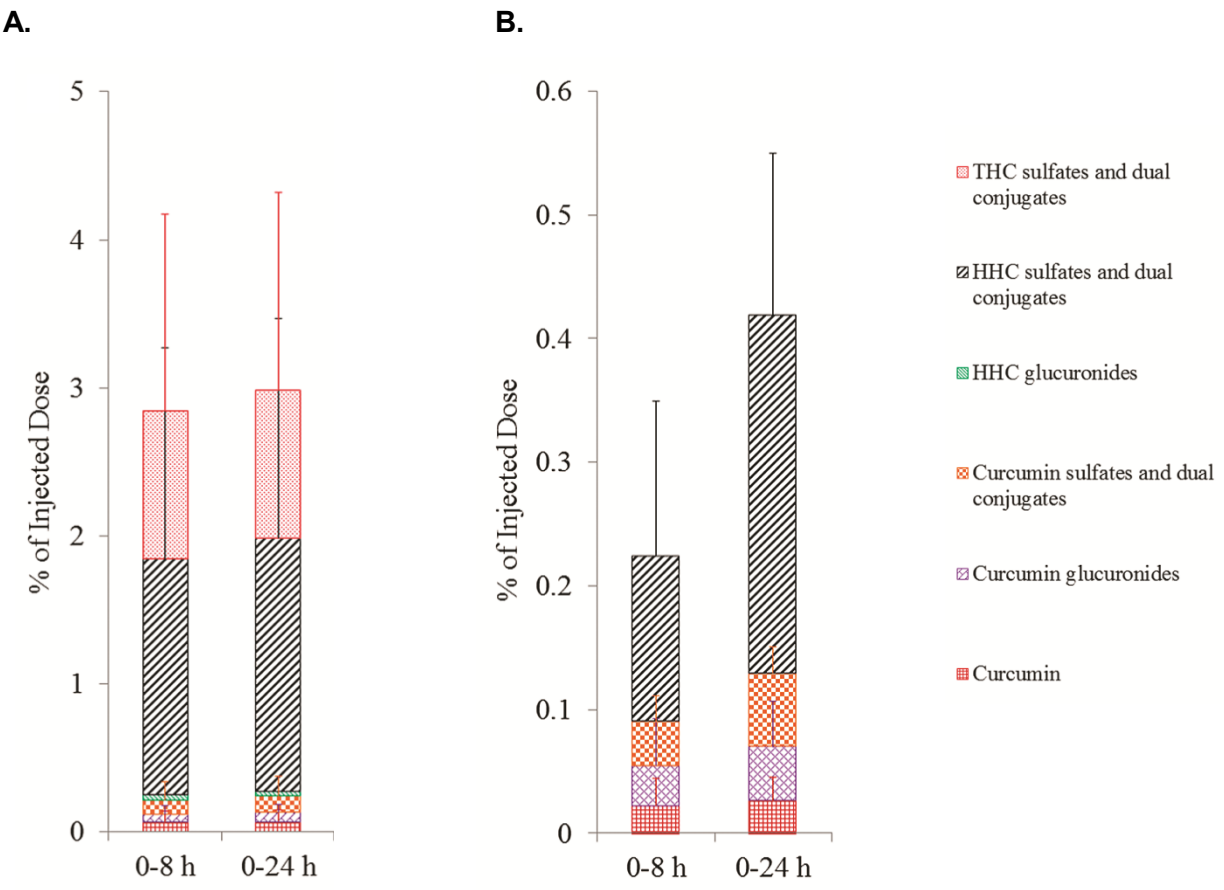

Figure V-9. Cumulative urinary excretion of curcumin and its metabolites after i.v. administration of (A) nanocurcumin (equivalent to 10 mg/kg curcumin) and (B) solvent solubilized curcumin (10 mg/kg) to S-D rats. Data are mean ± SD, n = 5 rats. Urine samples were collected at 0-8 and 8-24 h intervals. The %ID of curcumin and metabolites in bile was calculated as:

$$\frac{(\text{curcumin or metabolite molar concentration} \times \text{volume of collected urine})}{\text{Total molar dose}} \times 100\%$$

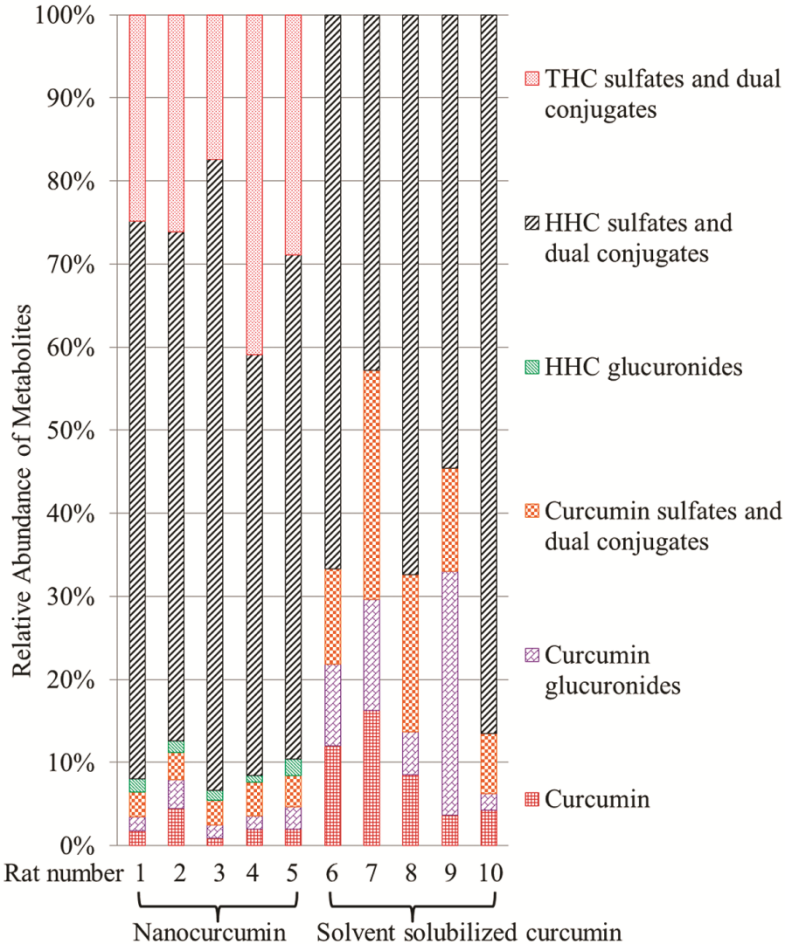

Figure V-10. Relative abundance of curcumin and its metabolites excreted into urine 0-24 h post i.v. administration of nanocurcumin (equivalent to 10 mg/kg curcumin) to rat 1-5 and solvent solubilized curcumin (10 mg/kg) to rat 6-10. The relative abundance of curcumin or metabolites in urine was calculated as:

$$\frac{\text{The molar amount of curcumin or individual metabolite in urine}}{\text{The sum of molar amount of curcumin and metabolites in urine}} \times 100\%$$

Tissue Distribution

Tissue distribution data of curcumin and its metabolites for the nanocurcumin (Figure V-11A) and solvent solubilized curcumin groups (Figure V-11B) are presented as %ID. Consistent with the above main plasma PK study, 6.6 ± 0.5% and 0.05 ± 0.05% of injected dose was detected as curcumin in plasma at 15 min postdose for the nanocurcumin and solvent solubilized curcumin groups, respectively. At 15 min postdose, 0.3 ± 0.1% (nanocurcumin group) and 0.07 ± 0.006% (solvent solubilized curcumin group) of the injected dose was detected in plasma as vanillylidenacetone (degradation product of curcumin), suggesting that degradation of curcumin in the blood circulation was very limited. Vanillylidenacetone was not detected in other tissues. No significant accumulation of nanoformulated curcumin in lung, spleen, heart and kidneys was observed (Figure V-11A). Surprisingly, 58.3 ± 4.4% of the injected solvent solubilized curcumin accumulated in lung at 15 min postdose (Figure V-11B), while only 0.3 ± 0.05% of injected nanocurcumin distributed in lung at the same time point. Hence, the nanoformulation changed tissue distribution of curcumin and prevented curcumin accumulation in the lung. For both groups, HHC and THC conjugates were not detected, and curcumin was the dominate analyte in lung, spleen, heart and kidneys. In contrast, HHC conjugates were dominant in liver at 15 min postdose for both groups. Overall, the nanoformulation changed tissue distribution of curcumin and decreased the relative abundance of metabolites in plasma, but did not significantly change the relative metabolite-to-curcumin ratios in major organs.

Figure V-11 also shows the changes in curcumin concentrations in plasma, lung, liver, spleen, heart and kidneys between 15-60 min. For the solvent solubilized curcumin group, the dramatic decrease in curcumin concentrations in plasma, spleen, heart and kidney over the 60 min time period suggests rapid elimination of curcumin. In contrast, for the nanocurcumin group, changes in curcumin concentrations were not observed in plasma, lung, heart and kidneys, suggesting a fraction of stable nanoparticles in these organs that protected curcumin from metabolism. For the nanocurcumin group, the curcumin concentration in spleen and liver increased from 15 min to 60 min, possibly due to release of curcumin from phagocytosed nanoparticles.

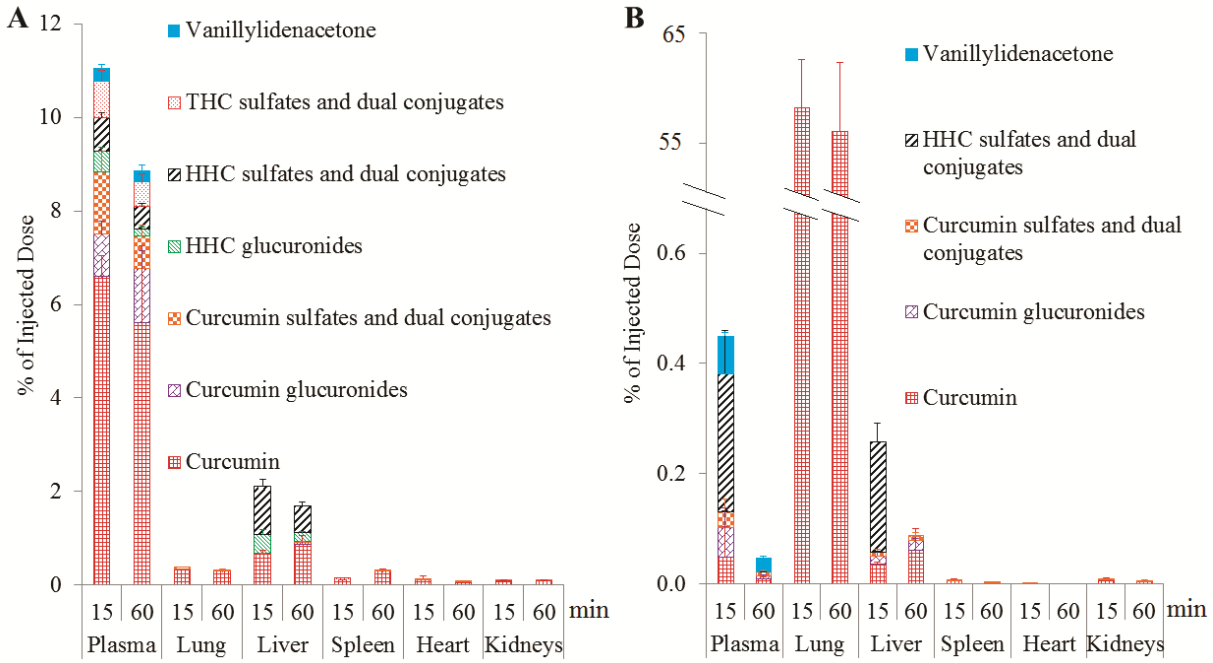

Figure V-11. Biodistribution of curcumin and its metabolites 15 min and 60 min post i.v. administration of (A) nanocurcumin (equivalent to 10 mg/kg curcumin) and (B) solvent solubilized curcumin (10 mg/kg) to S-D rats. Data are mean ± S.D., n = 3 rats. Plasma and tissue samples were collected at 15 min and 60 min postdose. The %ID of curcumin and metabolites in plasma was calculated as: (curcumin or metabolite molar concentration × total plasma volume) /total molar dose × 100%. The %ID of curcumin and metabolites in tissues was calculated as:

$$\frac{\text{(curcumin or metabolite molar concentration x tissue mass)}}{\text{Total molar dose}} \times 100\%$$

Analysis & Conclusions

In this study, we evaluated the effects of polymeric nanoparticle entrapment of curcumin on plasma pharmacokinetics, metabolite profile, biliary and urinary excretion, and tissue distribution, and further utilized metabolite profiles to estimate in vivo release. Consistent with previous nanoparticle studies [15, 33], nanocurcumin increased the plasma curcumin C_{max} by 1749-fold in comparison to solvent solubilized curcumin. The most likely explanation for the increase in nanocurcumin plasma concentration relative to solvent solubilized curcumin, is circulation of an encapsulated curcumin fraction (approx. 8% of the injected dose) which is not subjected to hepatic metabolism. Nanocurcumin also increased the plasma C_{max} of phase II metabolites by 4.0-9.9 fold. The low amount of encapsulated curcumin in circulation coupled with the high metabolite concentrations could have several possible causes, including nanoparticle accumulation in tissues, rapid degradation of curcumin, or burst release of curcumin.

Tissue distribution studies did not reveal significant accumulation of curcumin in lung, liver, spleen, heart and kidneys 15 and 60 min postdose of nanocurcumin (Figure V-11A). Furthermore, only 0.3 ± 0.1% of administered nanoformulated curcumin decomposed into vanillylidenacetone in plasma at 15 min postdose, suggesting that the rapid elimination of nanoformulated curcumin from plasma was not due to curcumin degradation. Suggestive of burst release, biliary excretion studies showed that 17.8 ± 3.9% of the injected dose was excreted into bile mainly as metabolites at 1 h postdose. Since only released curcumin can be metabolized, the detection of significant amounts of early metabolites in bile, urine and plasma supports a burst release mechanism. Burst release of the unaccounted for nanocurcumin fraction (>90%ID) would provide high concentrations of free curcumin for hepatic metabolism. In comparison, due to accumulation of a large portion of solvent solubilized curcumin dose in tissues (i.e. ~60 % lung), a relatively smaller fraction of unaccounted for solvent solubilized curcumin (~40%) is potentially available for metabolism. Due to uncertainty in the estimation of free curcumin available for metabolism in the solvent solubilized and nanocurcumin groups, a relationship between free curcumin and metabolism data cannot be determined, and we are unable to draw conclusions regarding the absolute extent and profile of the curcumin release from nanocurcumin. However, the low amount of circulating nanocurcumin (8% ID) and relatively high plasma, biliary and urinary metabolites, suggests rapid release of a substantial fraction of the encapsulated curcumin.

The altered lung and spleen distribution observed for nanocurcumin deserves further comment. Approximately 60% of the solvent solubilized curcumin accumulated in the lung, while lung accumulation of nanoformulated curcumin was not observed. Consistently, accumulation of curcumin in the lung has been reported previously in rats [2] and mice [34] following i.v. administration of free curcumin. Although solvent solubilized curcumin did not aggregate in rat plasma, curcumin may still precipitate upon interaction with red blood cells, and these particles could then accumulate in lung due to the narrow vasculature. The time-dependent accumulation of curcumin in the spleen, observed only in the nanocurcumin group, likely resulted from phagocyte uptake of unreleased nanoparticle-entrapped curcumin. Interestingly, nanocurcumin altered biliary and urinary metabolite profiles. Nanocurcumin exhibited higher biliary excretion of curcumin and glucuronides relative to other biliary metabolites. The increase in biliary curcumin may have resulted from saturation of the P450 enzymes following burst release. Alternatively, a previous study reported biliary excretion of 36% and 16% of parenterally administered 50 nm and 500 nm diameter polymeric nanoparticles, respectively, over a 24h period [35]. Correspondingly, biliary excretion of nanoparticles containing encapsulated curcumin might also account for the increase in the relative percentage of curcumin in bile. The increased urinary

curcumin excretion for nanocurcumin is more likely due to high systemic curcumin exposure and not excretion of encapsulated curcumin, as nanoparticles with a hydrodynamic diameter over 5.5 nm are unable to be eliminated through urinary excretion [36]. Since hepatic UGTs appear to have a very high capacity for curcumin glucuronidation [37], they are less likely to be temporarily saturated by the burst released curcumin in comparison to hepatic sulfotransferases (SULTs). This might explain the increase in the relative abundance of glucuronides in bile following burst release. Indeed, in vitro studies in which curcumin was incubated with rat liver subcellular fractions at a high micromolar concentration [38], resulted in greater formation of glucuronide (980 ± 150 nmol/mg protein) than sulfate conjugates (182 ± 39 nmol/mg protein). The greater relative abundance of curcumin and curcumin conjugates in urine for solvent solubilized curcumin (Figure V-9), may simply be explained by the higher LOQ for THC in comparison to curcumin (2500 vs. 20 ng/mL, respectively) (Table V-4) resulting in an inability to detect THC metabolites in the solvent solubilized curcumin group.

In summary, this study highlights the importance of in vivo drug release on the ADME of nanoformulated lipophilic drugs. Curcumin burst release from the polymeric nanoparticles increased biliary and urinary excretion of both curcumin and metabolites, but did not change the dominant elimination pathways. While nanocurcumin increased the relative abundance of curcumin and glucuronides in bile, urine and tissue metabolite profiles were not dramatically altered. Although the burst release observed in this study is a limitation for targeted tumor delivery, nanocurcumin still exhibits major advantages over solvent solubilized curcumin, as the nanoformulation does not result in lung accumulation and increases overall systemic curcumin exposure.

REFERENCES

1. Yallapu, M.M., Jaggi, M., and Chauhan, S.C., Curcumin nanoformulations: a future nanomedicine for cancer. *Drug Discov Today*, **2012**, 17(1-2), 71-80.
2. Ben, P., Liu, J., Lu, C., Xu, Y., Xin, Y., Fu, J., Huang, H., Zhang, Z., Gao, Y., Luo, L., and Yin, Z., Curcumin promotes degradation of inducible nitric oxide synthase and suppresses its enzyme activity in RAW 264.7 cells. *Int Immunopharmacol*, **2011**, 11(2), 179-186.
3. Binion, D.G., Heidemann, J., Li, M.S., Nelson, V.M., Otterson, M.F., and Rafiee, P., Vascular cell adhesion molecule-1 expression in human intestinal microvascular endothelial cells is regulated by PI 3-kinase/Akt/MAPK/NF-kappaB: inhibitory role of curcumin. *Am J Physiol Gastrointest Liver Physiol*, **2009**, 297(2), G259-268.
4. Jiang, W., Kou, J., Yuan, S., Sun, L., and Yu, B., A simplified and high-throughput chromogenic assay for testing tissue factor-dependent procoagulant activity. *J Biomol Screen*, **2011**, 16(3), 295-302.
5. Shah, V.O., Ferguson, J.E., Hunsaker, L.A., Deck, L.M., and Vander Jagt, D.L., Natural products inhibit LPS-induced activation of pro-inflammatory cytokines in peripheral blood mononuclear cells. *Nat Prod Res*, **2010**, 24(12), 1177-1188.
6. Sompamit, K., Kukongviriyapan, U., Nakmareong, S., Pannangpetch, P., and Kukongviriyapan, V., Curcumin improves vascular function and alleviates oxidative stress in non-lethal lipopolysaccharide-induced endotoxaemia in mice. *Eur J Pharmacol*, **2009**, 616(1-3), 192-199.
7. Sun, D., Zhuang, X., Xiang, X., Liu, Y., Zhang, S., Liu, C., Barnes, S., Grizzle, W., Miller, D., and Zhang, H.G., A novel nanoparticle drug delivery system: the anti-inflammatory activity of curcumin is enhanced when encapsulated in exosomes. *Mol Ther*, **2010**, 18(9), 1606-1614.
8. Zhao, C., Cai, Y., He, X., Li, J., Zhang, L., Wu, J., Zhao, Y., Yang, S., Li, X., Li, W., and Liang, G., Synthesis and anti-inflammatory evaluation of novel mono-carbonyl analogues of curcumin in LPS-stimulated RAW 264.7 macrophages. *Eur J Med Chem*, **2010**, 45(12), 5773-5780.
9. Zhao, C., Yang, J., Wang, Y., Liang, D., Yang, X., Li, X., Wu, J., Wu, X., Yang, S., and Liang, G., Synthesis of mono-carbonyl analogues of curcumin and their effects on inhibition of cytokine release in LPS-stimulated RAW 264.7 macrophages. *Bioorg Med Chem*, **2010**, 18(7), 2388-2393.
10. Murakami, R., Kambe, F., Mitsuyama, H., Okumura, K., Murohara, T., Niwata, S., Yamamoto, R., and Seo, H., Cyclosporin A enhances interleukin-8 expression by inducing activator protein-1 in human aortic smooth muscle cells. *Arterioscler Thromb Vasc Biol*, **2003**, 23(11), 2034-2040.
11. Vanaudenaerde, B.M., Wuyts, W.A., Geudens, N., Dupont, L.J., Schoofs, K., Smeets, S., Van Raemdonck, D.E., and Verleden, G.M., Macrolides inhibit IL17-induced IL8 and 8-isoprostane release from human airway smooth muscle cells. *Am J Transplant*, **2007**, 7(1), 76-82.
12. Chueh, S.C., Lai, M.K., Liu, I.S., Teng, F.C., and Chen, J., Curcumin enhances the immunosuppressive activity of cyclosporine in rat cardiac allografts and in mixed lymphocyte reactions. *Transplant Proc*, **2003**, 35(4), 1603-1605.
13. Bisht, S., Mizuma, M., Feldmann, G., Ottenhof, N.A., Hong, S.M., Pramanik, D., Chenna, V., Karikari, C., Sharma, R., Goggins, M.G., Rudek, M.A., Ravi, R., and Maitra, A., Systemic administration of polymeric nanoparticle-encapsulated curcumin (NanoCurc)

blocks tumor growth and metastases in preclinical models of pancreatic cancer. *Mol Cancer Ther*, **2010**, 9(8), 2255-2264.
14. Pramanik, D., Campbell, N.R., Das, S., Gupta, S., Chenna, V., Bisht, S., Sysa-Shah, P., Bedja, D., Karikari, C., Steenbergen, C., Gabrielson, K.L., and Maitra, A., A composite polymer nanoparticle overcomes multidrug resistance and ameliorates doxorubicin-associated cardiomyopathy. *Oncotarget*, **2012**, 3(6), 640-650.
15. Bisht, S., Mizuma, M., Feldmann, G., Ottenhof, N.A., Hong, S.M., Pramanik, D., Chenna, V., Karikari, C., Sharma, R., Goggins, M.G., Rudek, M.A., Ravi, R., Maitra, A., and Maitra, A., Systemic administration of polymeric nanoparticle-encapsulated curcumin (NanoCurc) blocks tumor growth and metastases in preclinical models of pancreatic cancer. *Mol Cancer Ther*, **2010**, 9(8), 2255-2264.
16. Wang, Y.J., Pan, M.H., Cheng, A.L., Lin, L.I., Ho, Y.S., Hsieh, C.Y., and Lin, J.K., Stability of curcumin in buffer solutions and characterization of its degradation products. *J Pharm Biomed Anal*, **1997**, 15(12), 1867-1876.
17. Vareed, S.K., Kakarala, M., Ruffin, M.T., Crowell, J.A., Normolle, D.P., Djuric, Z., and Brenner, D.E., Pharmacokinetics of curcumin conjugate metabolites in healthy human subjects. *Cancer Epidemiol Biomarkers Prev*, **2008**, 17(6), 1411-1417.
18. Pan, M.H., Huang, T.M., and Lin, J.K., Biotransformation of curcumin through reduction and glucuronidation in mice. *Drug Metab Dispos*, **1999**, 27(4), 486-494.
19. Bansal, S.S., Goel, M., Aqil, F., Vadhanam, M.V., and Gupta, R.C., Advanced drug delivery systems of curcumin for cancer chemoprevention. *Cancer Prev Res (Phila)*, **2011**, 4(8), 1158-1171.
20. Tsai, Y.M., Chien, C.F., Lin, L.C., and Tsai, T.H., Curcumin and its nano-formulation: the kinetics of tissue distribution and blood-brain barrier penetration. *Int J Pharm*, **2011**, 416(1), 331-338.
21. Cartiera, M.S., Ferreira, E.C., Caputo, C., Egan, M.E., Caplan, M.J., and Saltzman, W.M., Partial correction of cystic fibrosis defects with PLGA nanoparticles encapsulating curcumin. *Mol Pharm*, **2010**, 7(1), 86-93.
22. Shahani, K., Swaminathan, S.K., Freeman, D., Blum, A., Ma, L., and Panyam, J., Injectable sustained release microparticles of curcumin: a new concept for cancer chemoprevention. *Cancer Res*, **2010**, 70(11), 4443-4452.
23. Onoue, S., Takahashi, H., Kawabata, Y., Seto, Y., Hatanaka, J., Timmermann, B., and Yamada, S., Formulation design and photochemical studies on nanocrystal solid dispersion of curcumin with improved oral bioavailability. *J Pharm Sci*, **2010**, 99(4), 1871-1881.
24. Murugan, P. and Pari, L., Effect of tetrahydrocurcumin on plasma antioxidants in streptozotocin-nicotinamide experimental diabetes. *J Basic Clin Physiol Pharmacol*, **2006**, 17(4), 231-244.
25. Pfeiffer, E., Hoehle, S.I., Walch, S.G., Riess, A., Solyom, A.M., and Metzler, M., Curcuminoids form reactive glucuronides in vitro. *J Agric Food Chem*, **2007**, 55(2), 538-544.
26. Stern, S.T., Hall, J.B., Yu, L.L., Wood, L.J., Paciotti, G.F., Tamarkin, L., Long, S.E., and McNeil, S.E., Translational considerations for cancer nanomedicine. *J Control Release*, **2010**, 146(2), 164-174.
27. Letchford, K. and Burt, H.M., Copolymer micelles and nanospheres with different in vitro stability demonstrate similar paclitaxel pharmacokinetics. *Mol Pharm*, **2012**, 9(2), 248-260.
28. Stern, S.T., Zou, P., Skoczen, S., Xie, S., Liboiron, B., Harasym, T., Tardi, P., Mayer, L.D., and McNeil, S.E., Prediction of Nanoparticle Prodrug Metabolism by Pharmacokinetic Modeling of Biliary Excretion. *J Control Release*, **2013**, 172(2), 558-567.

29. Ireson, C., Orr, S., Jones, D.J., Verschoyle, R., Lim, C.K., Luo, J.L., Howells, L., Plummer, S., Jukes, R., Williams, M., Steward, W.P., and Gescher, A., Characterization of metabolites of the chemopreventive agent curcumin in human and rat hepatocytes and in the rat in vivo, and evaluation of their ability to inhibit phorbol ester-induced prostaglandin E2 production. *Cancer Res*, **2001**, 61(3), 1058-1064.
30. Asai, A. and Miyazawa, T., Occurrence of orally administered curcuminoid as glucuronide and glucuronide/sulfate conjugates in rat plasma. *Life Sci*, **2000**, 67(23), 2785-2793.
31. Davies, B. and Morris, T., Physiological parameters in laboratory animals and humans. *Pharm Res*, **1993**, 10(7), 1093-1095.
32. Li, X. and Cong, H., Platelet-derived microparticles and the potential of glycoprotein IIb/IIIa antagonists in treating acute coronary syndrome. *Tex Heart Inst J*, **2009**, 36(2), 134-139.
33. Mohanty, C. and Sahoo, S.K., The in vitro stability and in vivo pharmacokinetics of curcumin prepared as an aqueous nanoparticulate formulation. *Biomaterials*, **2010**, 31(25), 6597-6611.
34. Gao, Y., Li, Z., Sun, M., Li, H., Guo, C., Cui, J., Li, A., Cao, F., Xi, Y., Lou, H., and Zhai, G., Preparation, characterization, pharmacokinetics, and tissue distribution of curcumin nanosuspension with TPGS as stabilizer. *Drug Dev Ind Pharm*, **2010**, 36(10), 1225-1234.
35. Jani, P.U., Nomura, T., Yamashita, F., Takakura, Y., Florence, A.T., and Hashida, M., Biliary excretion of polystyrene microspheres with covalently linked FITC fluorescence after oral and parenteral administration to male Wistar rats. *J Drug Target*, **1996**, 4(2), 87-93.
36. Moghimi, S.M., Hunter, A.C., and Andresen, T.L., Factors controlling nanoparticle pharmacokinetics: an integrated analysis and perspective. *Annu Rev Pharmacol Toxicol*, **2012**, 52, 481-503.
37. Hoehle, S.I., Pfeiffer, E., and Metzler, M., Glucuronidation of curcuminoids by human microsomal and recombinant UDP-glucuronosyltransferases. *Mol Nutr Food Res*, **2007**, 51(8), 932-938.
38. Ireson, C.R., Jones, D.J., Orr, S., Coughtrie, M.W., Boocock, D.J., Williams, M.L., Farmer, P.B., Steward, W.P., and Gescher, A.J., Metabolism of the cancer chemopreventive agent curcumin in human and rat intestine. *Cancer Epidemiol Biomarkers Prev*, **2002**, 11(1), 105-111.

ABBREVIATIONS

%ID	percentage of injected dose
AAALAC	Association for Assessment and Accreditation of Laboratory Animal Care
AA	acrylic acid
ABN	abnormal
ADME	absorption, distribution, metabolism, excretion
APTT	activated partial thromboplastin time
AUC	area under the curve
BLOQ	below limit of quantitation
C_{max}	concentration maximum
CI	confidence interval
CV	coefficient of variation
CVF	cobra venom factor
DLS	dynamic light scattering
DMPK	drug metabolism & pharmacokinetics
DMSO	dimethyl sulfoxide
EPR	enhanced permeability and retention
ESI-MS	electrospray ionization mass spectrometry
EU	endotoxin unit
FBS	fetal bovine serum
h	hour
HepG2	human hepatocarcinoma cells
HHC	hydrotetracurcumin
HuLA	human leukocyte activation
IC_{50}	inhibitory concentration, 50%
ICCVAM	Interagency Coordinating Committee on the Validation of Alternative Methods
IS	internal standard
ITA	immunotoxicity assay
i.v.	intravenous
LAL	Limulus Amoebocyte Lysate
LC-MS	liquid chromatography-mass spectrometry
LDH	lactate dehydrogenase
LLC-PK1	porcine renal proximal tubule cell line
LOQ	limit of quantitation
LPS	lipopolysaccharide
min	minute
MRT	mean residence time
MS	mass spectrometry
MTT	3-(4,5-dimethylthiazol-2-yl)-2,5-diphenyltetrazolium bromide
NC	negative control
NCI	National Cancer Institute
NCL	Nanotechnology Characterization Laboratory
NIPAAM	N-isopropylacrylamide
NK	natural killer cells
NTP	National Toxicology Program
PBS	phosphate buffered saline
PC	positive control

PCC	physicochemical characterization
PHA-M	Phytohemaglutinin-M
PdI	polydispersity index
PT	prothrombin time
QC	quality control
RE	relative error
RPT	rabbit pyrogen test
RSD	relative standard deviation
RSD	relative standard deviation
RT-CES	real-time cell electronic sensing
s.c.	subcutaneous
S-D	Sprague Dawley
SD	standard deviation
SE	standard error
S/N	signal-to-noise
STE	sterility
THC	tetrahydrocurcumin
USP	United States Pharmacopeia
Vd_{ss}	volume of distribution, steady state
VP	vinylpyrrolidone

Nanotechnology Characterization Laboratory

Scott E. McNeil
Anil K. Patri
Stephan T. Stern
Marina A. Dobrovolskaia
Pavan Adiseshaiah
Jeffrey D. Clogston
Girija Chaubey
Jennifer B. Hall
Rachael M. Crist
Chris McLeland
Tim Potter
Barry Neun
Sarah Skoczen
Sonny Man
Matt Hansen
Jamie Rodriguez

Electron Microscopy Laboratory

Ulrich Baxa
Anne Kamata
Sarah Anderson

Pathology/Histotechnology Laboratory

Diana Haines
Gloryvee Rivera
Melissa Orr
Wendi Custer

Small Animal Imaging Program

Joseph Kalen
Marcelino Bernardo
Lilia Ileva

Laboratory Animal Sciences Program

Dan Logsdon

This project has been funded in whole or in part with federal funds from the National Cancer Institute, National Institutes of Health, under contract HHSN261200800001E. The content of this publication does not necessarily reflect the views or policies of the Department of Health and Human Services, nor does mention of trade names, commercial products, or organizations imply endorsement by the U.S. Government.